Advanced Drug Delivery Reviews 138 (2019) 211–232

Contents lists available at ScienceDirect

Advanced Drug Delivery Reviews

journal homepage: www.elsevier.com/locate/addr

Physically-triggered nanosystems based on two-dimensional materials for cancer theranostics

Ding-Kun Ji, Cécilia Ménard-Moyon, Alberto Bianco *

CNRS, Immunology, Immunopathology and Therapeutic Chemistry, University of Strasbourg, UPR 3572, Strasbourg 67000, France

ARTICLE INFO

Article history:
Received 29 March 2018
Received in revised form 3 August 2018
Accepted 27 August 2018
Available online 31 August 2018

Keywords:
2D Materials
Nanomaterials
Graphene
Therapy
Diagnosis
Theragnosis

ABSTRACT

There is an increasing demand to develop effective methods for treating malignant diseases to improve healthcare in our society. Stimuli-responsive nanosystems, which can respond to internal or external stimuli are promising in cancer therapy and diagnosis due to their functionality and versatility. As a newly emerging class of nanomaterials, two-dimensional (2D) nanomaterials have attracted huge interest in many different fields including biomedicine due to their unique physical and chemical properties. In the past decade, stimuli-responsive nanosystems based on 2D nanomaterials have been widely studied, showing promising applications in cancer therapy and diagnosis, including phototherapies, magnetic therapy, drug and gene delivery, and non-invasive imaging. Here, we will focus our attention on the state-of-the-art of physically-triggered nanosystems based on graphene and two-dimensional nanomaterials for cancer therapy and diagnosis. The physical triggers include light, temperature, magnetic and electric fields.

Contents

* Corresponding author.
E-mail address: a.bianco@ibmc-cnrs.unistra.fr (A. Bianco).

https://doi.org/10.1016/j.addr.2018.08.010
0169-409X/

1. Introduction

Developing simple, effective, and reliable methods to treat diseases is an important way to improve healthcare in our society. The development of new drug delivery methods will have a significant effect on the drug theranostic (combination of therapy and diagnosis) efficacy [1]. However, conventional drug administration procedures generally require a high dose to achieve therapeutic levels at the pathological sites, leading to various undesired effects, such as toxicity to normal cells and tissues, and often multidrug resistance [2,3]. To improve the theranostic efficiency, various novel drug delivery systems have been successfully explored to enhance drug accumulation at the disease sites as well as to minimize side effects. This is possible with the help of nanotechnology and has confirmed to be effective by some preclinical studies [4,5].

Stimuli-responsive nanosystems are specialized nanosized systems that can adjust to surrounding environments, manage transport of ions and molecules, change wettability and adhesion of different species under stimuli, or convert chemical and biochemical signals into optical, electrical, thermal and mechanical signals, and *vice versa* [6]. They provide a new horizon in the development of nanosystems for many biomedical uses. In general, these stimuli can be divided into two modes: i) internal stimuli including temperature, pH, redox potential and enzymes; and ii) external stimuli comprising light, surrounding temperature, electric field, magnetic field, radiofrequency and ultrasounds [3,7]. Owing to the high local concentration, reduced overall injection dose, and reduced systemic toxicity, these stimuli-responsive nanosystems pave a new way for personalized medicine [8]. Until now, many types of nanomaterials have been used to construct stimuli-responsive nanosystems for therapy and diagnosis, such as polymers [9,10], carbon materials [11–13], and inorganic metal nanoparticles (NPs) [14,15].

As a newly emerging class of nanomaterials, 2D nanomaterials (Fig. 1) have aroused increasing interest since the discovery of exfoliated graphene in 2004, which led to the Nobel Prize in Physics in 2011 [16–18]. In addition to graphene nanosheets, other graphene-like 2D materials, such as transition metal dichalcogenides (TMDs), transition metal oxides, graphitic carbon nitride (g-C_3N_4), hexagonal boron nitride (hBN), 2D clays like layered double hydroxides and laponite™, black phosphorus (BP) monolayers, and MXene (*i.e.* Ti_3C_2, Ti_2C, Ta_4C_3, *etc.*) monolayers, have attracted extensive attention in various fields including nanoelectronic devices, transparent conductors, energy, and catalysis [19].

2D nanomaterials are highly diverse in terms of mechanical, chemical, and optical properties as well as size, shape, biocompatibility, and biodegradability. These various characteristics make them interesting nanomaterials for biomedical applications, including drug and gene delivery, bioimaging, biosensing, and cancer therapies [20,21]. 2D nanomaterials possess the highest specific surface area of all known materials. Therefore, they can adsorb various types of molecules including drugs, proteins, nucleic acids, fluorescent probes with high efficiency through covalent or non-covalent interactions and enable superior controlled release by external stimuli (Fig. 2) [12,22]. Simultaneously, a range of functional NPs, such as iron oxide NPs (IONPs), Au NPs, and inorganic quantum dots, can be adsorbed onto the surface of 2D nanomaterials to endow them with additional characteristics like magnetism, radioactivity, electrochemical properties, *etc.* In addition, 2D

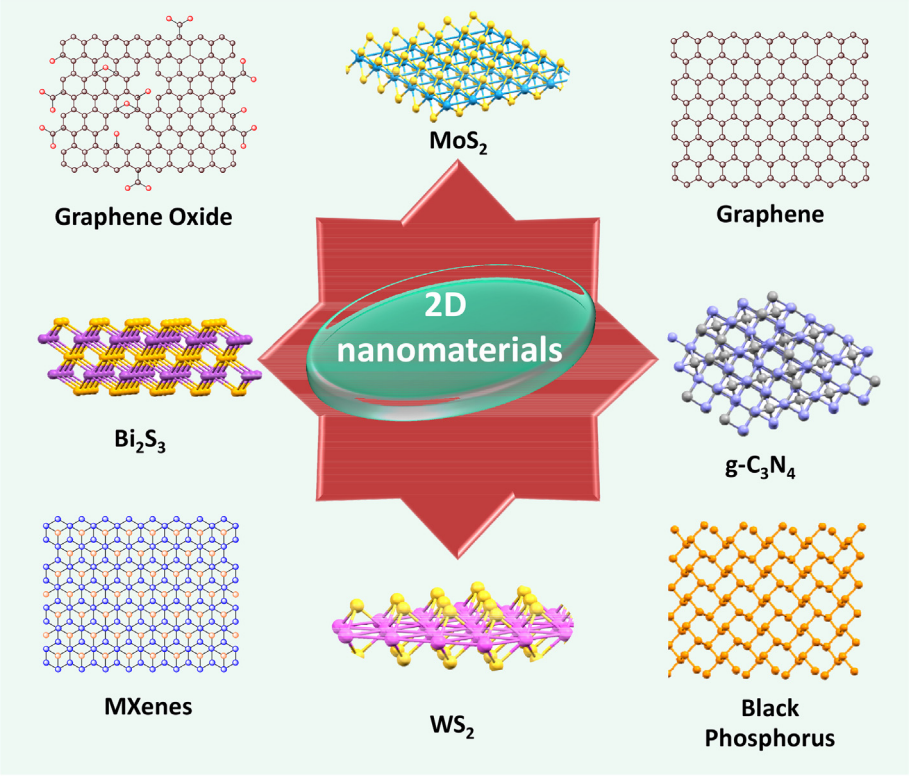

Fig. 1. Illustration of 2D nanomaterials including graphene, graphene oxide (GO), MoS_2, WS_2, g-C_3N_4, Bi_2S_3, black phosphorus, and MXenes.

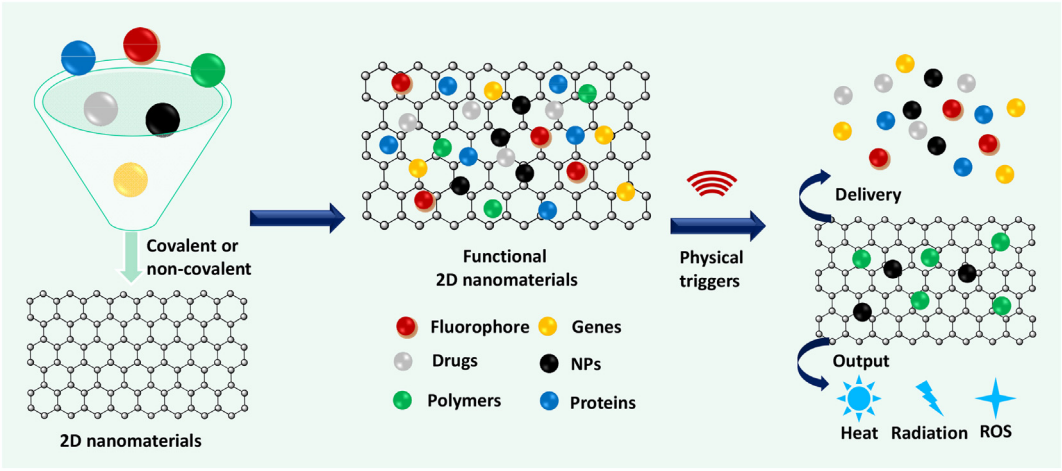

Fig. 2. Schematic diagram for the design of physically-triggered nanosystems.

nanomaterials typically have ultrathin structure and can respond to light, which is useful in optical therapies, including photothermal therapy (PTT) and photodynamic therapy (PDT) [23]. Considering these characteristics, 2D materials were demonstrated to be excellent platforms for theranostic uses [24].

Recently, a certain number of review articles focusing on the applications of 2D nanomaterials in biosensing, phototherapies, and imaging have appeared [25–28]. However, 2D nanomaterial research in biomedical field is still at its early stage of maturation. Here, we focus our attention on physically-triggered nanosystems for therapy and diagnosis based on graphene and other 2D nanomaterials. The physical stimuli include light, temperature, magnetic and electric fields (Fig. 3).

This review will assess the state-of-the-art developments of physically-triggered nanosystems for therapy and diagnosis. The design

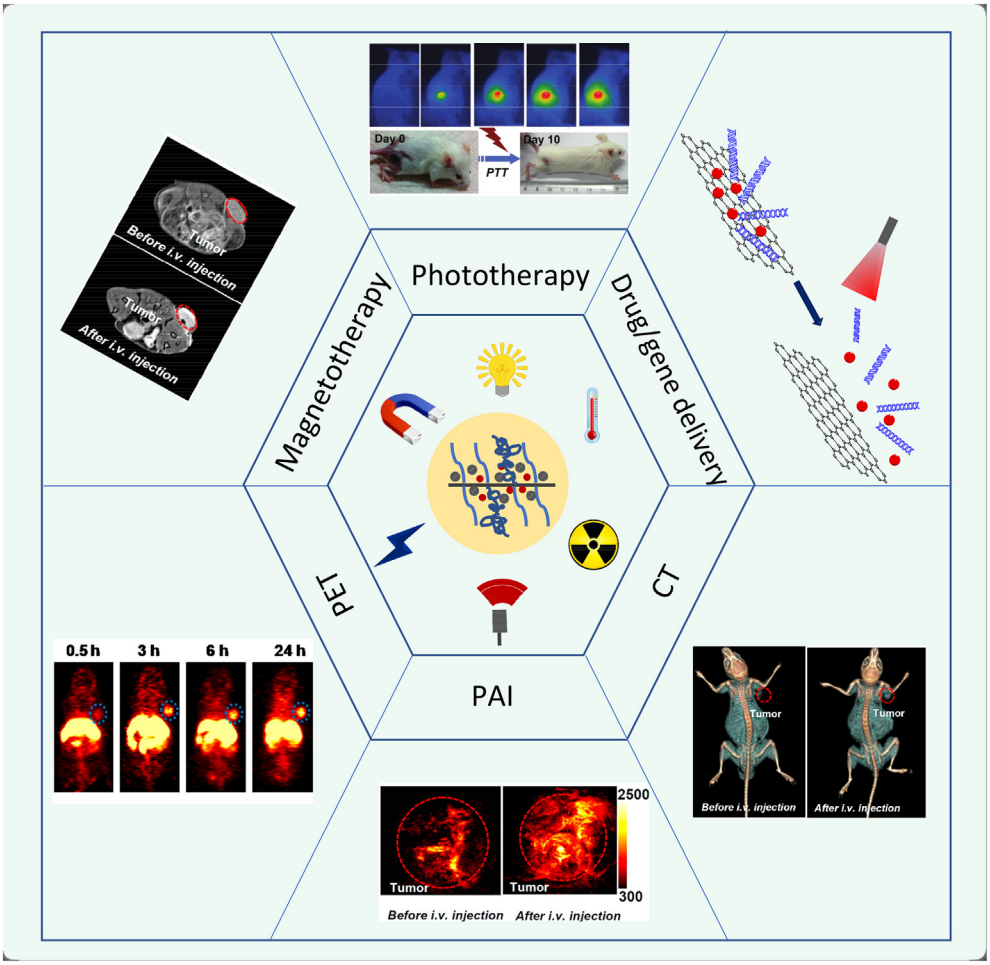

Fig. 3. Different physical triggers exploited for nanosystems based on 2D materials in therapy and diagnosis, including magnetic induction, light irradiation, temperature, electric field. PET (positron emission tomography), PAI (photoacoustic imaging), CT (X-ray computed tomography). Optical imaging pictures are adapted from Cheng et al. [29], Liu et al. [30]. Both of them copyright 2015 American Chemical Society.

and working mechanisms of each physically-triggered nanosystem will be discussed in dedicated sections. Finally, the challenges and future directions, development and exploitation of physically-triggered nanosystems based on 2D materials will be highlighted.

2. Graphene-based nanosystems for therapy and diagnosis

Graphene, with its atomically thin, honeycomb lattice that consists of sp^2 -hybridized carbons, exhibits remarkable electronic, thermal, optical, and mechanical properties [16]. As a novel nanocarbon material, graphene and its derivative GO have received much attention in materials science and biotechnology. Significant progress has been made in the use of graphene in biosensing [31,32], drug delivery [33,34], PTT/PDT [35], and imaging [36]. Graphene-based materials have been developed as physically-triggered nanosystems (Table 1) for therapy and diagnosis due to the following reasons: 1) their high specific surface area results in π-stacking interactions with the aromatic rings of drugs and photosensitizers (PSs) as well as hydrophobic forces, suggesting that graphene can be used as carrier to release payloads to the target sites; 2) due to the oxygenated functional groups, GO and reduced GO (rGO) can adsorb not only many drugs by electrostatic interactions and hydrogen bonding, but also other molecules to offer additional optical and magnetic properties, which could be useful to provide contrast for *in vivo* multimodal imaging; 3) owing to high photothermal conversion efficiency, graphene possesses high ability to transfer the absorbed radiation into thermal energy. The resulting temperature change at the target site usually causes structural damages to cells and intracellular proteins leading to cell death.

2.1. Light-triggered nanosystems for therapy and diagnosis

Among external stimuli, light is the most flexible and can be used as a safe and useful energy source. Light irradiation is particularly interesting because intensity and wavelength can be easily tuned [35,37]. UV,

Table 1
Physically-triggered nanosystems based on graphene for therapy and diagnosis.

Graphene-based materials	Payloads	Physical trigger	Therapy	Imaging modes	*In vitro* models	*In vivo* models	Refs.
PEG-GO	Cy7	Light	PTT	FI	/	Mice bearing 4T1 tumor	[42]
PEG-rGO	RGD, Cy5	Light	PTT	FI	U87MG cells	/	[44]
rGONM-PEG	RGD, Cy7	Light	PTT	FI	U87MG cells	Mice bearing U87MG tumor	[45]
PEG-GO	ZnPc	Light	PDT	/	MCF-7 cells	/	[52]
FA-GO	Ce6	Light	PDT	/	MGC-803 cells	/	[53]
HA-GO	Ce6	Light	PDT	/	HeLa cells	/	[54]
GO-mAb	PPa	Light	PDT	/	U87MG cells	/	[56]
PEG-GO	DOX	Light/pH	PTT/drug delivery	/	EMT6 cells	Mice bearing EMT6 tumor	[58]
PAH-GO	DOX	Light	Drug delivery	/	/	/	[60]
PEG-BPEI-rGO	DOX	Light/pH/GSH	Drug delivery	/	PC-3 and HeLa cells	/	[61]
rGO-PEG	Resveratrol	Light	Drug delivery	/	4T1 cells	Mice bearing 4T1 tumor	[62]
GO-PEG-PEI	Polo-like kinase 1	Light	Gene delivery	/	MDA-MB-435s cells	/	[65]
PEG-BPEI-rGO	pDNA	Light	Gene delivery	/	PC-3 and NIH/3T3 cells	/	[66]
PEG-GO	Ce6	Light	PTT/PDT	/	KB cells	/	[67]
NGO-PEG-DA	DOX	Light/pH	PTT/drug delivery	/	MCF-7/WT and MCF-7/ADR cells	/	[68]
rGO-lactoferrin	DOX	Light	PTT/drug delivery	FI	RG2 cells and MRC-5 cells	Mice bearing RG2 tumor	[69]
GO-silica-peptide	DOX	Light/pH	PTT/drug delivery	/	U251 glioma cells	/	[70]
PEG-GO/CuS	DOX	Light	PTT/drug delivery	/	HeLa cells	Mice bearing HeLa cells	[72]
GO@Ag-PEG	DOX	Light	PTT/drug delivery	X-ray imaging	MCF-7 cells	S180 tumor-bearing mice	[73]
rGO-AuNRVe	DOX	Light/pH	PTT/drug delivery	PAI, PET	U87MG cells	Mice bearing U87MG tumor	[74]
GO/PNIPAM	/	Temperature/pH	/	/	/	/	[80]
PNIPAM-GS hydrogel	CPT	Temperature/pH	Drug delivery	/	A-5RT3 cells	/	[81]
GO-PNP	DOX	Temperature	Drug delivery	/	HepG2 cells	/	[83]
GO-Fe_3O_4	DOX	Magnetic	Drug delivery	/	SK3 cells	/	[86]
GO-Fe_3O_4-FA	DOX	Magnetic	Drug delivery	/	HeLa cells	/	[87]
GN-CNT-Fe_3O_4	5-Fluorouracil	Magnetic	Drug delivery	/	HepG2 cells	/	[88]
$ZnFe_2O_4$-rGO	/	Magnetic/light	PTT	/	U87MG cells	/	[89]
GO-Fe_3O_4	MTX and CPT	Magnetic/light	PTT/drug delivery	/	HepG2 cells	HepG2 tumor bearing mice	[90]
Aminodextran-GO-Fe_3O_4	/	Magnetic	/	MRI	HeLa cells	/	[92]
rGO-Fe_3O_4-PEG	/	Magnetic/light	PTT	MRI, PAI, FI	4T1 cells	4T1 tumor bearing mice	[93]
GO-Fe_3O_4-PEG	DOX	Magnetic/light	Drug delivery/PTT	MRI	4T1 cells	4T1 tumor bearing mice	[94]
GO-Fe_3O_4-Au-PEG	/	Magnetic/light	PTT	MRI, X-ray imaging	4T1 cells	4T1 tumor bearing mice	[95]
Fe_3O_4-GO	5-Fluorouracil	Magnetic	Drug delivery	MRI	/	/	[96]
GO-DTPA-Gd	DOX	Magnetic	Drug delivery	MRI, FI	HepG2 cells	/	[97]
GO-Fe_3O_4-PEG	/	Magnetic/light	PTT	DW-MRI	4T1 cells	4T1 tumor bearing mice	[98]
GO/Fe_3O_4/PEI gel	DOX	Magnetic	MHT/drug delivery	FI	MCF-7 cells	S180 tumor-bearing mice	[99]
Polymer-GO-Fe_3O_4	DOX or paclitaxel	Magnetic	MHT/drug delivery	/	MCF-7 cells	MCF-7 tumor bearing mice	[100]
Fe_3O_4-GO	DOX	Magnetic/light	MHT/drug delivery/PTT	/	HeLa cells	HeLa tumor bearing mice	[101]
PMAA-graphene gel	DOX	Electric	Drug delivery	/	/	CD-1 mice	[104]
GO-PPy	Dexamethasone	Electric	Drug delivery	/	Hippocampal cells	/	[105]
rGO-HA gel	Methyl orange	Electric	Drug delivery	/	/	/	[106]
Fe_3O_4/MnO-GO	DOX	Magnetic, pH, redox	MHT/drug delivery	MRI	MDA-MB-231 cells	4T1 tumor bearing mice	[107]

visible, or near-infrared (NIR) regions of the light spectrum can be all used to trigger drug or gene release from appropriately designed nanosystems [38,39]. Among them, NIR is the best choice for applications in the biomedical field due to its better transmission through the tissues (penetration in the tissue of about 10 cm). In addition, NIR causes less damage to cells than UV and visible light, because hemoglobin, water, and lipids barely absorb light in this region [40]. In the following section, we will selectively discuss light-triggered drug delivery and light-triggered therapies based on PTT and PDT using graphene.

2.1.1. Photothermal therapy using graphene

PTT is a powerful technology, which employs photoabsorbing agents to generate heat from appropriate light irradiation, leading to thermal ablation of cells. Ideal photothermal agents should exhibit strong absorbance in the NIR, which is a transparent window for biological tissues, and efficiently convert the absorbed energy into heat [41]. In addition, the agents used in PTT should be non-toxic and possess high tumor accumulation ability to improve the therapeutic efficacy. To date a range of inorganic and organic photothermal agents including graphene have been developed for PTT in cancer research.

In 2010 Yang et al. reported the first success of using polyethylene glycol (PEG)-modified GO (PEG-GO) for efficient *in vivo* PTT on mice bearing 4T1 tumor cells [42]. The authors observed that this nanoconjugate (10–50 nm lateral size) possessed a strong NIR absorbance. After intravenous (i.v.) injection, high tumor accumulation of PEG-GO was obtained due to the enhanced permeability and retention (EPR) effect in tumor tissues. Under NIR laser irradiation (at 808 nm), the surface temperature of the tumors reached ~50 °C, leading to efficient tumor ablation. Following the reduction of GO leading to partial restoration of the aromatic and conjugated character of graphene, it was found that PEGylated rGO exhibited 6-fold higher NIR absorption than PEG-GO. The mass extinction coefficient for PEG-rGO at 808 nm was 24.6 $L \cdot g^{-1} \cdot cm^{-1}$, nearly twice that of gold nanorods [43]. After attaching the targeting Arg-Gly-Asp (RGD) peptide to PEG-rGO, the conjugate was taken up by human glioblastoma U87MG cancer cells with high selectivity. When exposed to 808 nm irradiation, U87MG cells were completely destroyed within 8 min [44]. To further improve the photothermal conversion efficiency of graphene, some graphene-based nanomaterials with new structures were designed and fabricated. For example, Akhavan et al. fabricated a 2D rGO nanomesh (rGONM) *via* photocatalytic degradation of rGO [45]. The rGONM has abundant uniform pores (~8 nm) on its surface. After functionalization with PEG, this rGONM exhibited about 4.2- and 22.4-fold higher NIR absorption at 808 nm than PEG-rGO and PEG-GO. Following the modification with the RGD peptide and cyanine 7 (Cy7), this multi-functional rGONM was utilized for *in vivo* tumor targeting and fluorescence imaging (FI) of U87MG tumors. After intravenous injection of a low concentration (10 $\mu g \cdot mL^{-1}$) of conjugate and exposure to low laser power (0.1 $W \cdot cm^{-2}$) irradiation, this nanosystem was able to induce a complete tumor ablation.

2.1.2. Photodynamic therapy using graphene

PDT is an optical non-invasive treatment modality that uses appropriate laser light to activate exogenous PSs inside the target cells, resulting in the formation of reactive oxygen species (ROS) such as singlet oxygen ($^1O_2$) or free radicals that ultimately lead to cell apoptosis and/or necrosis [39,46]. PDT is especially suitable for epithelial tumors, such as skin or breast tumors because they are easily reached by visible and NIR light. PDT has obtained regulatory approval for clinical applications in various diseases, like age-related macular degeneration [47], psoriasis [48], and some oncological diseases [49,50]. A wide range of PS molecules, most of which containing porphyrin structures, have been combined with graphene and applied in PDT. In GO-based PDT nanosystems, GO usually plays the role of platform for high PS loading due to its water dispersibility and extremely high specific surface area, allowing to improve accumulation of PSs in tumor site. Moreover, due to its broad absorption spectrum from 200 to 1000 nm, GO can quench the fluorescence and phototoxicity of PSs *via* energy transfer during the blood circulation (in normal vasculature) [51]. The complex remains stable and keeps the phototoxicity of PSs "off" until it is activated by stimuli resulting in desorption of the PS molecules from graphene. GO-based smart nanosystems can remotely control the photoactivity of PSs and have the potential to be ideal carriers of PSs that do not work until they reach the site of action (*i.e.*, tumor sites), leading to minimum damage to healthy tissues and blood cells.

In 2010 Dong et al. designed the first PDT nanosystem containing graphene by loading the photosensitizer zinc phthalocyanine (ZnPc) on the surface of a PEGylated GO *via* π-stacking and hydrophobic interactions [52]. Compared to other photosensitizer carriers such as polymeric micelles and silica NPs, PEGylated GO showed a higher photosensitizer loading efficiency. Under irradiation by a Xe light, this nanosystem led to a lethal effect on human MCF-7 breast cancer cells within 5 min. To increase the accumulation of PSs at the tumor site, Huang et al. designed and prepared folic acid (FA)-conjugated GO as drug delivery system for targeted PDT [53]. In this work, chlorin e6 (Ce6) was loaded on FA-modified GO *via* hydrophobic interactions and π-stacking. Ce6 was released from GO thanks to acidic pH in lysosomes (pH 4–5). The FA-GO-Ce6 could specifically target human stomach cancer MGC-803 cells causing approximately 90% loss of viability under irradiation at 633 nm, demonstrating a high photodynamic efficacy. Li et al. constructed hyaluronic acid (HA)-GO conjugates with a high loading of Ce6 for PDT [54]. In this work, the activity of Ce6 adsorbed onto HA-GO was mostly switched off in aqueous solution to ensure biocompatibility, but it was quickly recovered after its release from the carrier surface upon cellular uptake. Under irradiation at 670 nm, the PDT efficiency of the HA-GO/Ce6 nanohybrid was 10 times higher than that of free Ce6 in HeLa cells.

Beside these promising results, some challenges still exist in photosensitizer delivery. Among them, phototoxicity to normal cells is one of the most urgent issue that needs to be solved. Undesired delivery usually makes the photosensitizer to stay in the skin and the eyes several days and even weeks. The ROS induced by the PSs can damage the vascular system causing burns, swelling, pain and other serious side effects [55]. To reduce these effects, Wei et al. developed a phototoxicity on/off nanosystem by attaching pyropheophorbide-a (PPa) and a monoclonal antibody (mAb) targeting the integrin $\alpha_v\beta_3$, on GO surface [56]. Due to π–π interactions between PPa and GO, the phototoxicity of PPa was switched off in aqueous solutions. When this nanosystem was in non-aqueous environment, the π–π interactions between PPa and GO were broken leading to recovery of the phototoxicity of PPa. *In vitro* results demonstrated that this nanosystem displayed low toxicity (off-state) into cytoplasm, but when in contact with mitochondria, it penetrated into them. In this lipid environment, the phototoxicity was turned "on" (on-state) to generate $^1O_2$ to kill cancer cells. This targeting system improved the PS pharmacokinetics and ultimately enhanced the treatment outcome with low side effects (Fig. 4).

2.1.3. Light-triggered nanosystems for drug and gene delivery

Since Dai's group first reported that graphene can be used for drug delivery [57], a range of 'smart' systems based on this material have been designed to increase the release of anticancer drugs and reduce side effects in cancer treatment. Among them, light-triggered drug delivery nanosystems have attracted tremendous interest due to several advantages. These advantages include: 1) the mild photothermal effect (43–45 °C) caused by light that has the capacity to increase the permeability of the cell membrane accumulating more nanomaterials in tumor region [58,59]; 2) the photothermal effect (photoinduced local heat generation) that can change the binding energy between graphene and the drugs, leading to rapid and substantial drug release upon NIR light; and 3) the photothermal effect that has the ability to induce the structural degradation of the carriers or the vesicles leading to enhanced drug release.

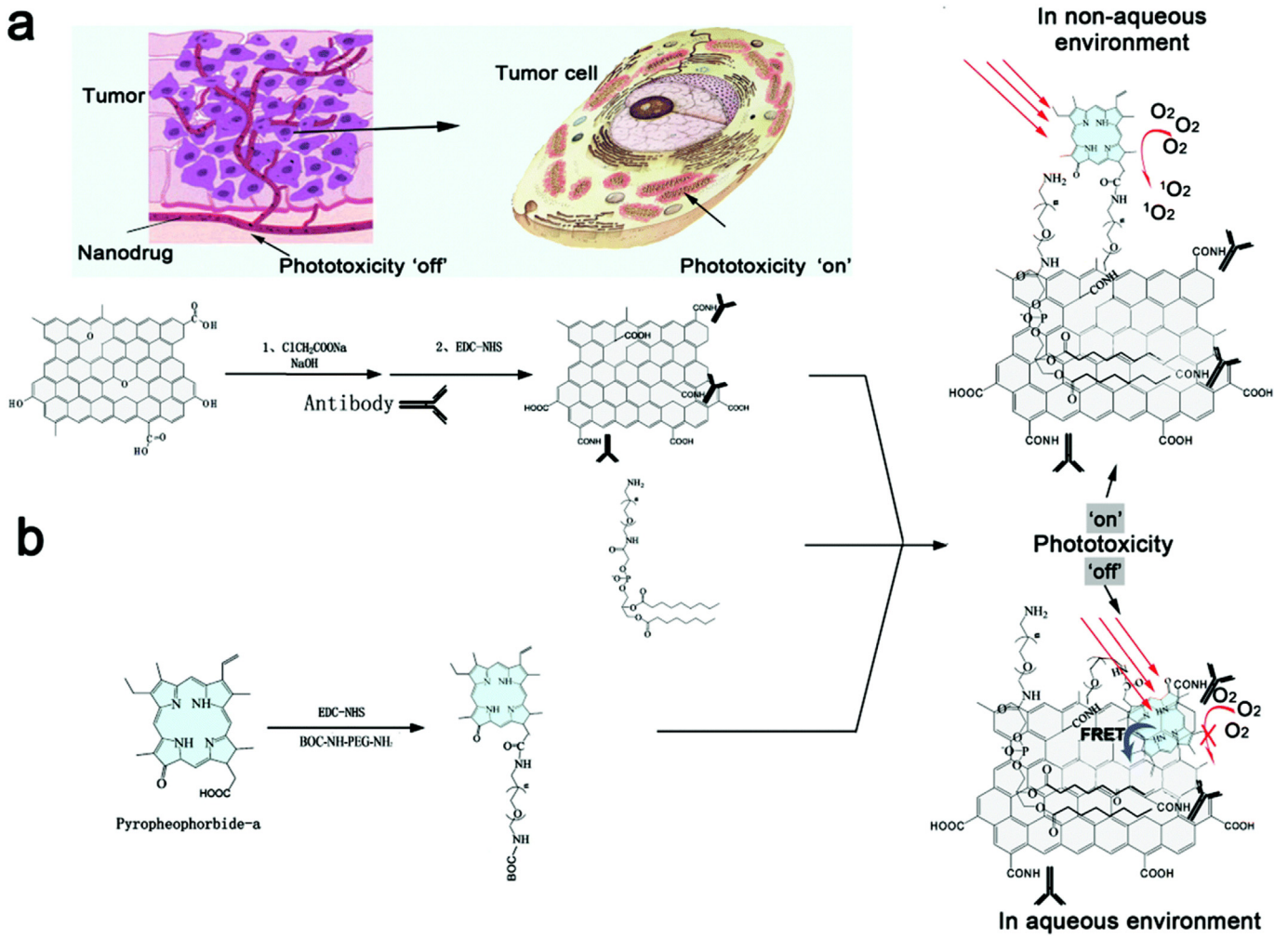

Fig. 4. The synthesis and action procedure of PPa-GO-mAb. (a) Use of PPa-GO-mAb showing phototoxicity switching when mitochondria are targeted. (b) Scheme of the synthesis of PPa-GO-mAb and its two states in different environments. Adapted from Wei et al. [56]. Copyright 2016 Royal Society of Chemistry.

In 2012, Kurapati et al. developed NIR-light responsive GO-poly (allylamine hydrochloride) (PAH) capsules and demonstrated the release of the encapsulated anticancer drug doxorubicin (DOX) [60]. These capsules possessed a high and broad absorption (400–1200 nm). Upon irradiation with a NIR laser (at 1064 nm) for 45 s, the capsules were completely ruptured by the heat locally generated by the irradiation. Simultaneously almost 85% of DOX was released from the capsules proving the attractive properties of this system for on-demand drug delivery. In another approach, Kim et al. explored nanosized PEG-branched polyethyleneimine (BPEI)-rGO conjugate by covalently grafting rGO with BPEI and PEG to photothermally trigger cytosolic drug delivery [61]. The authors found that PEG-BPEI-rGO could release DOX, previously complexed to this system, to cancer cells under NIR laser irradiation. Moreover, with the help of GO-induced photothermally endosomal disruption and the proton sponge effect of BPEI, PEG-BPEI-rGO could easily escape the endosomes to kill more efficiently cancer cells. Similarly, Chen et al. developed a functionalized nanosized rGO-PEG with high loading of resveratrol (RV) for remotely NIR controlled drug delivery towards 4T1 breast cancer *in vitro* and *in vivo* [62]. The results showed that after cellular uptake, rGO-PEG-RV was encapsulated into the endosomes and then merged with lysosomes, which offered an endogenous acidic medium causing a slow RV release. Under NIR irradiation at 808 nm the photothermal effect of rGO-PEG-RV further promoted a rapid RV release (Fig. 5).

In the last decade, gene therapy has drawn great attention in both the academic world and industry. This therapeutic modality is expected to be an effective strategy for the treatment of cancers, cardiovascular diseases, viral infections, and other genetic dysfunctions [63]. As one of the non-viral carriers, GO has shown the highest gene loading due to the interactions between oligonucleotide fragments and its surface modified with appropriate polymers to complex nucleic acids [64]. Similar to the release mechanism of drugs, light irradiation can be also used as stimulus to remotely control the gene release. In 2013, Feng et al. found that the dual-polymer-functionalized GO conjugate (GO-PEG-PEI) showed good gene transfection efficiency [65]. Under a low power NIR laser irradiation, the mild photothermal heating could increase the cell membrane permeability to enhance the cellular uptake of GO-PEG-PEI. Moreover, the GO conjugate could serve as a NIR light controllable siRNA delivery platform to silence polo-like kinase 1 gene in human breast cancer cells (MDA-MB-435s cells). In another work, Kim et al. observed that PEG-BPEI-rGO had a high gene transfection efficiency without observable cytotoxicity in PC-3 and NIH/3 T3 cells [66]. Moreover, under NIR irradiation, locally induced heat could accelerate endosomal escape of PEG-BPEI-rGO, thus displaying enhanced gene transfection efficiency.

2.1.4. Light-triggered nanosystems for combined therapies

We already discussed that light-triggered nanosystems have remarkable potential in PTT to destruct tumors. However, PTT alone is unlikely to eradicate cancer cells at once because of the restricted phototreated area and depth-dependent heat in the tumor. To date, chemotherapy is still a major therapeutic approach for the treatment of a

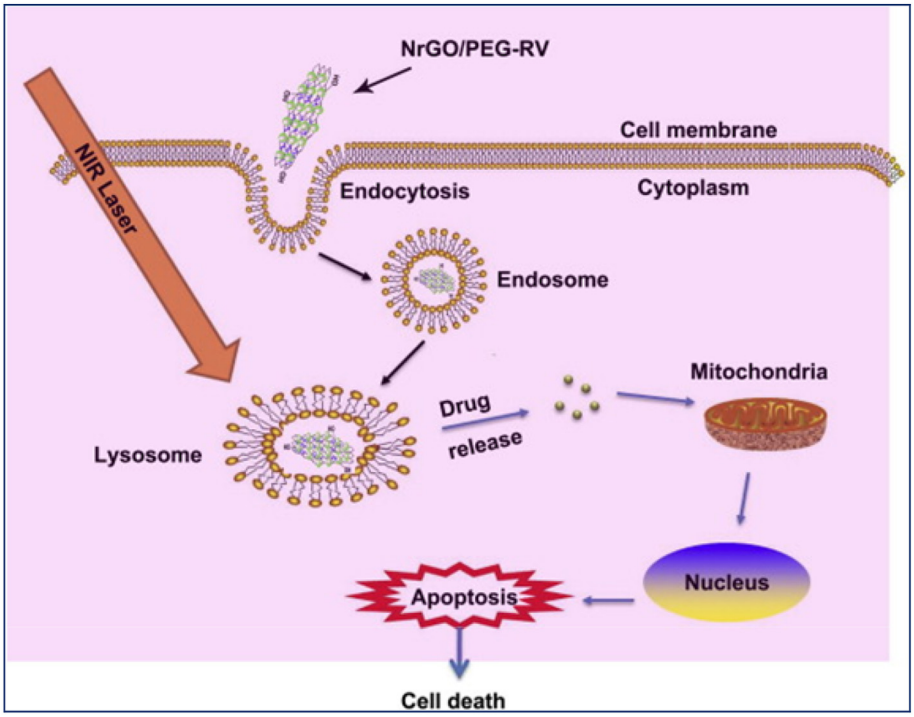

Fig. 5. Schematic illustration of photothermally controlled action mechanism of rGO-PEG-RV inducing cell death (NrGO stands for nanosized rGO). Adapted from Chen et al. [62]. Copyright 2014 Elsevier Ltd.

wide variety of cancers. Unfortunately, chemotherapy suffers from the low tumor uptake of the drugs, unavoidable side effects and multidrug resistance. In this context, combined therapies are able to complement limitations of individual therapies to achieve a better efficacy. Combined with PTT, light-triggered drug delivery has been employed in a wide range of cancer treatments, such as gene-photothermal synergistic therapy [65,66] or photodynamic-photothermal therapy [67], showing a better therapeutic response compared to mono-therapies.

Combined PTT-chemotherapy is an effective method to improve cancer treatment, because PTT can increase the sensitivity of chemotherapy and synergistically improve the therapeutic effects. Zhang et al. found that PEG-GO has a very high DOX loading capacity (142.5 wt%), which is far beyond other common drug carriers (generally below 100 wt%) [58]. Drug release from GO was triggered by both pH changes and NIR laser irradiation. After intratumoral (i.t.) injection of PEG-GO (devoid of DOX) and exposure to NIR irradiation, the temperature of the EMT6 tumor tissue increased to 50 °C. The combined chemo-photothermal treatment resulted in complete destruction of the EMT6 breast tumor *in vivo* without mice weight loss or tumor recurrence, superior to chemotherapy or photothermal treatment alone.

Combined PTT-chemotherapy can be also used to overcome drug resistance. Feng et al. developed a pH-responsive nanocarrier by conjugating nano-GO (NGO) with PEG and positively charged PAH, the latter subsequently modified with 2,3-dimethylmaleic anhydride (DA) [68]. The obtained conjugate was stable and negatively charged under physiological pH (7.4). Once in a slightly acidic pH (*e.g.* 6.8), it was rapidly converted into positively charged nanocarriers with markedly enhanced cellular uptake. After being loaded with DOX, the obtained NGO-PEG-DA/DOX responded to pH change of tumor microenvironment inducing an accelerated drug release under the cell lysosomal pH (5.0–5.5), especially in drug-resistant MCF-7/ADR cells. Taking advantage of the NIR absorbance of NGO and combination of PTT and chemotherapy, the system offered enhanced cell-killing ability for both wild-type MCF-7/WT cells and drug-resistant cancer MCF-7/ADR cells (Fig. 6).

Alternatively, Hu et al. developed a protein-graphene-protein (PGP) capsule using rGO and lactoferrin which exhibited precise on-demand drug release under highly controlled NIR irradiation [69]. This system displayed the capacity to effectively avoid the premature release of the cargo before it was induced by NIR light at the target site, therefore avoiding unintended side effects. Combined thermal-chemotherapy *in vivo* demonstrated that this nanosystem led to glioma tumor growth suppression not only in the phototreated area but also in the widely surrounding tumor cells, with little side effects (Fig. 7).

Recently, graphene-family nanomaterials have been used to form hybrids with mesoporous silica [70,71], CuS NPs [72], Ag NPs [73], and gold nanorods [74], in light-triggered nanosystems for combined therapy in many malignant tumors. The resulting rGO/GO hybrids usually displayed superior properties than rGO/GO alone, resulting in higher drug loading, stronger NIR absorption, and higher photothermal conversion efficiency. For example, Wang et al. prepared a targeting peptide-modified mesoporous silica-coated graphene nanosystem [70]. This complex adsorbed DOX with a high loading efficiency (about 127 wt%) and displayed a high absorption in the NIR window and an efficient heat transformation. Cytotoxicity experiments demonstrated that combined therapy triggered by NIR light provoked the highest rate of glioma cell death compared to that of single chemotherapy or PTT. Bai et al. developed PEG-GO/CuS by growing CuS NPs on PEG-GO surface for cervical cancer treatment [72]. The PEG-GO/CuS complex exhibited a high DOX loading efficiency (90 wt%) and an enhanced DOX release by NIR irradiation (at 980 nm). In a tumor-bearing mouse model, the chemo-photothermal effect of PEG-GO/CuS/DOX showed the ability to significantly inhibit mouse cervical tumor growth and avoid tumor recurrence.

2.2. Temperature-triggered nanosystems for therapy

Many diseases including tumors and inflammatory diseases typically lead to increased temperature in lesions (~40–42 °C) compared to normal tissue (~37 °C) [7,75]. Temperature differences between normal and tumor tissue have also been used to diagnose early-stage

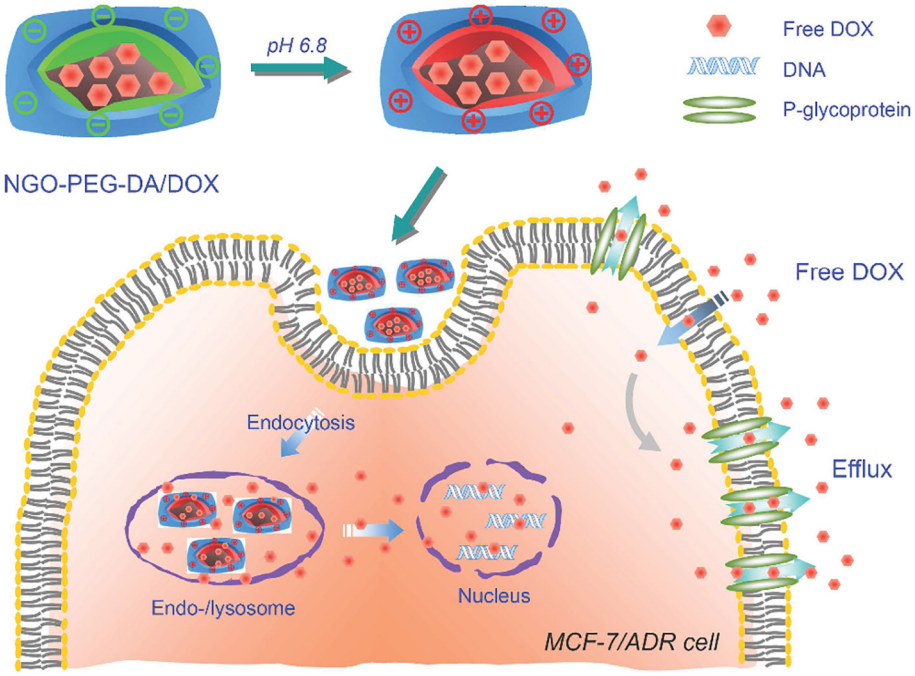

Fig. 6. Schematic illustration of the acidic extracellular environment-induced charge reverse of NGO-PEG-DA/DOX complex, its cellular uptake and intracellular acidic environment-triggered DOX release. Compared to wild-type MCF-7 cells (MCF-7/WT), drug-resistant MCF-7/ARD cells, with a higher expression of P-glycoprotein, showed a rapid drug efflux. Adapted from Feng et al. [68]. Copyright 2014 WILEY-VCH Verlag GmbH & Co.

tumors [76,77]. With the aim to exploit the spontaneous temperature of the tissues, a range of temperature-triggered nanosystems have been developed for drug delivery to tumor by modifying graphene with thermoresponsive polymers [11]. In this type of systems, graphene serves as carrier to load drugs, while the polymers with low critical solution temperature (LCST) serve as triggers responding to the temperature and inducing the release of drugs in the diseased tissues [78]. Ideally, a temperature-triggered nanosystem should retain the drugs at body temperature, and rapidly deliver them at the disease site by spontaneous hyperthermia [2,7].

As the best-known thermosensitive polymer, poly(*N*-isopropylacrylamide) (PNIPAM) and its derivatives have attracted constant attention in graphene-based temperature-triggered systems, since their corresponding LCST is about 32 °C, which is close to the physiological temperature of the human body [79]. PNIPAM-based graphene complexes have been investigated as carriers for drug delivery. Sun

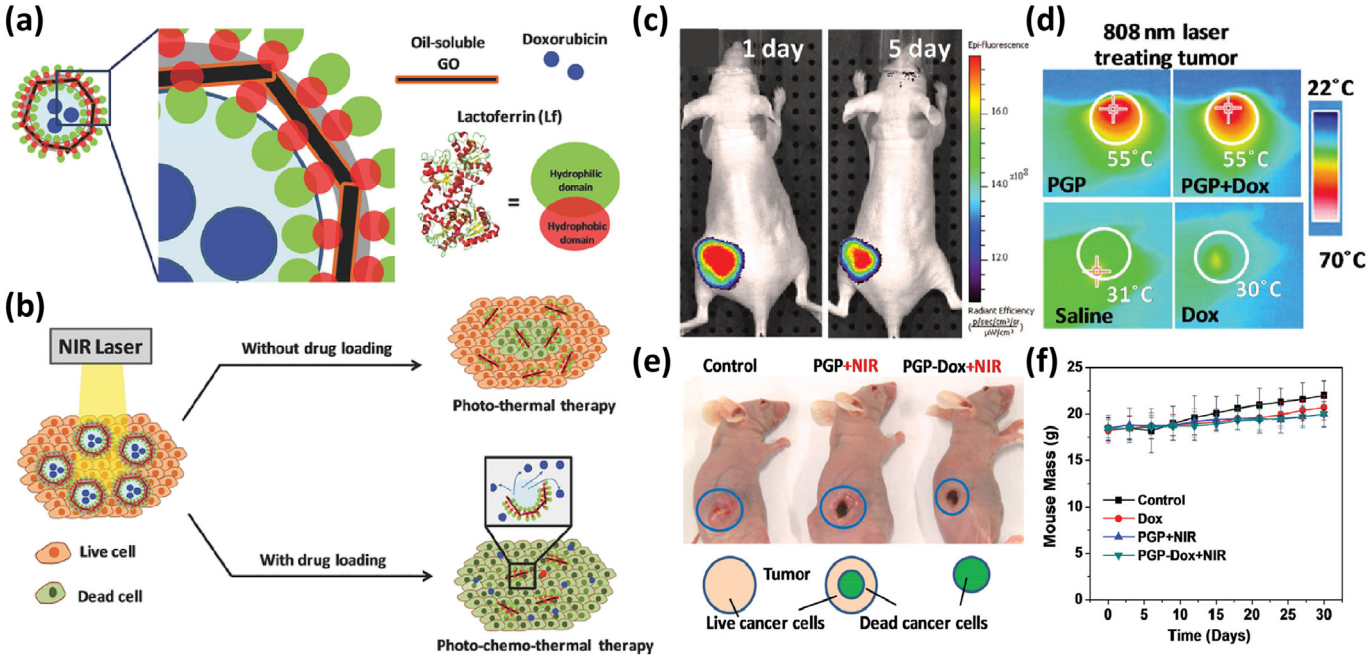

Fig. 7. (a) Schematic illustration of core–shell PGP capsules encapsulating DOX. (b) Under NIR irradiation, the PGP capsules with and without loading DOX exhibited different cell killing efficacy. (c) *In vivo* study of PGP capsules. Fluorescence images of RG2 tumor-bearing mice 1 and 5 days after intravenous injection of the PGP capsules. (d) Infrared thermal images of RG2 tumor-bearing mice under PGP + NIR treatment. (e) RG2 tumor treated by PGP + NIR light (middle) and PGP-DOX + NIR light (right) after 2 months. (f) Mouse weight as a function of post-treatment time displaying no weight loss for 30 days in all groups. Adapted from Hu et al. [69]. Copyright 2014 WILEY-VCH Verlag GmbH & Co.

et al. developed the first GO/PNIPAM hydrogel by covalently binding GO sheets and PNIPAM-co-acrylic acid microgels directly in water [80]. This hydrogel exhibited dual thermal and pH responses with good reversibility showing potential biological applications as carrier for controlled drug delivery. Unfortunately, *in vitro* and *in vivo* experiments to demonstrate the potential of this hydrogel have not been performed. In another work, Pan et al. functionalized graphene sheet (GS) with PNIPAM *via* click chemistry [81]. The resulting PNIPAM-GS exhibited a phase transition temperature at 33 °C and possessed a superior capability of binding camptothecin (CPT) with a loading ratio of 18.5 wt%, which is two times greater than that of PEG-NGO (PEG modified NGO) [57] and four times that of FA-NGO (folic acid-modified GO) [82]. The *in vitro* drug release experiments showed that 16.9% and 19.4% of CPT were released after 72 h at 37 °C in water and PBS, respectively, affording a strong potency to kill metastatic skin cancer cells. Wang et al. synthesized GO-PNP hybrids [PNP: PNIPAM-poly (ethylene oxide)] with different PNP coverage by assembling PNP on GO nanosheets [83]. The resulting GO-PNP exhibited a phase transition temperature at 34.8 °C, which is about 2.8 °C higher than that of the homopolymeric PNIPAM (32 °C). This synthesized hybrid displayed high DOX loading efficiency (~91 wt%). About 22% of DOX was released upon temperature change to 37 °C, achieving ~80% apoptosis of HepG2 cells.

These examples show that temperature-triggered nanosystems based on graphene have big potential application in cancer therapies. However, until now no temperature-triggered nanosystem has been used for *in vivo* applications as the LCST was always lower than that of the body temperature (37 °C). Therefore, further work needs to be done, such as modifying PNP to reach higher LCST.

2.3. Magnetic field-triggered nanosystems for therapy and diagnosis

Magnetic field is considered one of the best external stimuli compared to other stimuli such as light irradiation, ultrasound or electric field. Indeed, it permits no depth-penetration limit in the human body and remote-management without physical or chemical contact with the body [8,84]. Magnetic field mainly has three applications in the biomedical field including targeting transport, magnetic resonance imaging (MRI) and magnetothermal stimulation. Although graphene does not have paramagnetic characteristics, thanks to the large surface area and oxygen-containing active groups (in GO/rGO), a range of magnetic NPs (MNPs) have been adsorbed onto its surface resulting in various magnetic field-responsive nanosystems. So far, magnetic field-triggered nanosystems based on graphene have been used for many biomedical applications including magnetic targeting for drug delivery, magnetic hyperthermia (MHT), and MRI-guided therapy [85].

2.3.1. Magnetic field-triggered nanosystems for targeted drug delivery and photothermal therapy

Magnetic field is like a pair of “invisible hands”, which can move magnetic NPs to a target location. Magnetic field-responsive nanosystems possess an intrinsic ability to respond to an external field. Thus, magnetic targeting represents an alternative to commonly used passive targeting due to the EPR effect and positive targeting (*i.e.* by conjugation of FA or HA). When exposed to an external magnetic field, the responsive nanosystems can be magnetized, they can move thanks to magnetic driving forces and concentrate at specific sites [8]. Hence, this powerful tool has the ability to deliver drugs directly to target sites and maintain drug concentration during the treatment time, thus reducing side effects due to non-specific accumulation in normal tissues.

As the most widely used magnetic materials, Fe_3O_4 can be combined to graphene for targeted drug delivery due to its superparamagnetic properties, low toxicity, and favorable biocompatibility in physiological environments [85]. Yang et al. first prepared a superparamagnetic GO-Fe_3O_4 hybrid through chemical precipitation [86]. This nanohybrid had a high DOX loading capacity (108 wt%) and was further modified with folate to endow the hybrid with a double targeting ability (magnetic targeting and positive targeting). This multifunctional GO was quickly delivered into the targeted tumor cells SK3 cells, which overexpress folate receptors and show toxicity to HeLa cells after loading DOX [87]. This work provided a new strategy to improve targeted drug delivery and it also allowed the use of GO-Fe_3O_4 hybrid as an ideal drug carrier for tumor combination therapy. In parallel, Fan et al. developed a graphene nanosheet-carbon nanotube-iron oxide NP hybrid (GN-CNT-Fe_3O_4), which exhibited superparamagnetic properties that were exploited for magnetic targeting [88]. The hybrid was able to bind the anticancer drug 5-fluorouracil (5-FU) displaying a pH-activated 5-FU release profile to kill HepG2 cells. Because both graphene and Fe_3O_4-based nanoparticles were shown to absorb NIR light, it has been demonstrated that magnetic GO can be used as magneto-photothermal agents for targeted PTT [89] or combination of PTT with chemotherapy to treat cancers [90]. Shen et al. explored superparamagnetic GO-Fe_3O_4 conjugates, which can specifically deliver both CPT and methotrexate (MTX) to tumor site by the induction of an external magnetic field [90]. Combined with PTT under NIR irradiation, the multidrug synergistic delivery system displayed an enhanced capacity to effectively inhibit sarcoma tumor growth leading to necrosis.

2.3.2. MRI-guided cancer diagnosis and therapy

MRI is a powerful and widely used clinical diagnostic technology with high resolution and deep tissue penetration [15]. MNPs with unique magnetic properties are able to improve the signal-to-noise ratio in MRI and have been widely applied as MRI contrast agents (CAs). Under magnetic field, the MNPs not only can drive drugs to specific sites, but they can also act as CAs to assess the distribution of the molecules *in vivo* and to visualize the tumors and the circulatory system. Graphene-based MNPs with enhanced physiological stability have been widely used for MRI-guided cancer therapy and diagnosis including MRI-guided PTT and MRI-guided drug delivery.

Generally, MRI CAs are divided into two types: T_1 and T_2 CAs, depending on the signal enhancement or decay. Due to the presence of paramagnetic Fe^{3+} and its property of high saturation magnetization, Fe_3O_4 NPs are considered good candidates for T_2-weighted MRI. In 2010, Cong et al. firstly prepared a magnetic rGO by *in situ* high-temperature decomposition of Fe^{3+} magnetite NPs on the rGO sheets [91]. This work opened the prologue of graphene-based magnetic theranostic. To increase the physiological stability and reduce the cytotoxicity of the GO-based magnetic NPs, Chen et al. modified Fe_3O_4 with aminodextran on GO and successful applied them for cellular MRI tests [92]. Subsequently, Liu's group and others [93–96] developed a series of Fe_3O_4-modified graphene derivatives, which served as T_2-weighted MRI CAs. Combined with PTT and drug delivery (*i.e.* DOX or 5-Fu), these magnetic GO nanosystems can get cancer treatment and diagnosis together in a single platform showing the ability to monitor the progress of cancer treatment in real time with a big potential in clinical applications. As the most frequently employed T_1 CAs in clinics, paramagnetic gadolinium complexes were also used in combination with GO for MRI. Zhang et al. chemically conjugated diethylenetriaminepentaacetic acid (DTPA) to GO, followed by Gd(III) complexation, to form a T_1 MRI CA [97]. This complex exhibited significantly a higher r_1 relaxivity enhancement than the commercially used Magnevist™. This new MRI CA was internalized into cells, allowing cellular MRI, and simultaneously delivered DOX to lesions to kill HepG2 cells. Diffusion-weighted magnetic resonance imaging (DW-MRI) is a clinical imaging method which provides image contrast based on the differences in diffusion of water molecules. It is able to assess the extent of tissue damage after treatment by monitoring the apparent diffusion coefficient (ADC). Fu et al. used DW-MRI to monitor GO-mediated PTT under different conditions [98]. In this work, a GO-IONP-PEG conjugate was driven to the tumor site by a magnetic field. After NIR irradiation for 5 min, the temperature of the tumor tissue increased from 34.5 °C to

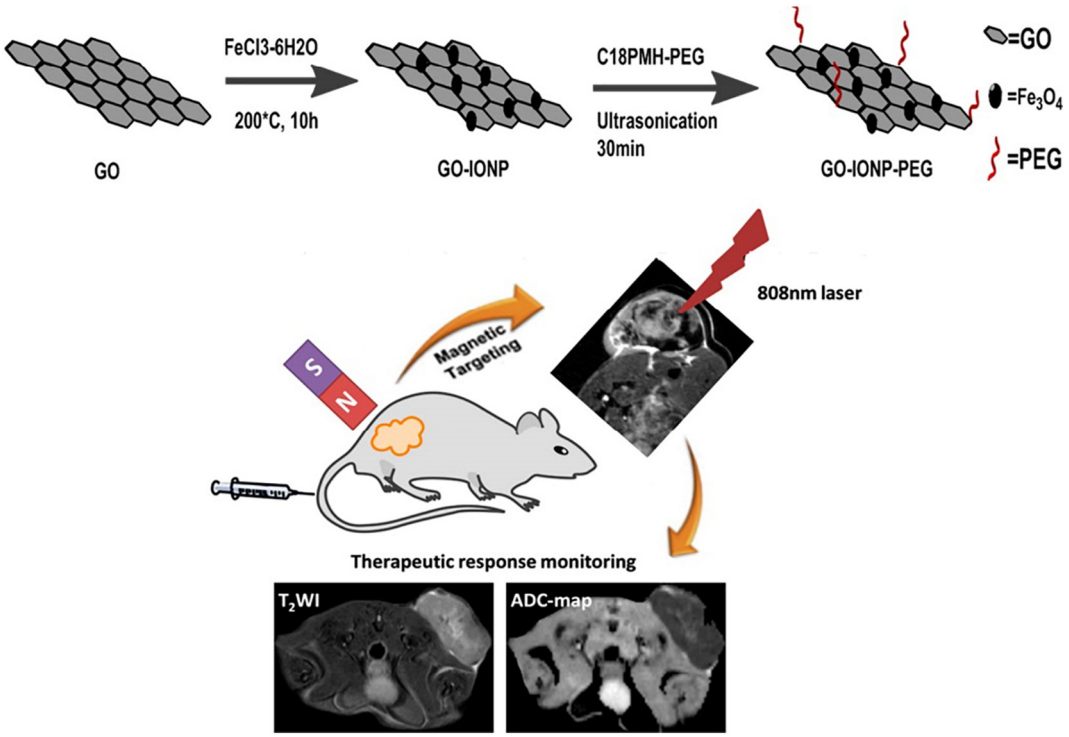

Fig. 8. Schematic illustration of experimental design. GO-IONP-PEG was prepared by PEGylation of IONP-deposited GO nanosheets. GO-IONP-PEG was systematically administered into tumor-bearing animals. The tumor targeting could be facilitated by an external magnetic field applied to the tumor area. Under photoirradiation, the GO-IONP-PEG mediated PTT was inflicted on cancer cells. The therapy response was monitored by both T_2-weighted MRI and DW-MRI. Reprinted from Fu et al. [98] Copyright 2016 American Chemical Society.

65.2 °C leading to complete 4T1 breast cell ablation. After PTT, the animals were scanned by DW-MRI at different time points and the mean ADC value changes in tumors were monitored. The result showed an increase of the ADC value (>80%) within 48 h which associated with effective tumor growth suppression and extended animal survival. This work suggested ADC as an effective early prognosis marker for PTT, showing a good prospect for future development and clinical translation of the technology (Fig. 8).

2.3.3. Magneto-thermal therapy

Magnetic hyperthermia is a new generation of tumor thermal therapy method triggered by an alternating magnetic field (AMF), which is associated to the unique ability of MNPs (with superparamagnetic behavior) to generate local heat to ablate cancer cells [15]. Compared to PTT, magnetic hyperthermia can target and penetrate deeply inside the biological systems. Moreover, the magnetic field does not cause adverse effect on biological tissues, which is distinctly beneficial for non-invasive *in vivo* applications [85]. Magneto-thermal therapy has been widely explored for cancer treatment. Zhu et al. created a magneto-induced drug delivery system made of a DOX-GO-Fe_3O_4-PEI gel for breast cancer treatment [99]. After exposure to an AMF of 488 kHz for 30 min, the increased temperature (7 °C) in tumor enhanced the release of DOX improving tumor treatment. At the same time, Swain et al. observed that GO modified with poly(vinyl alcohol) (PVA), polyvinylpyrrolidone (PVP), and Fe_3O_4 has the ability to load and release both hydrophobic and hydrophilic drugs [100]. Under an AMF of 250 kHz, it took <16 min for the polymer-GO-Fe_3O_4 to reach the stable hyperthermia temperature of 42 °C. This local generated heat was able to enhance the drug release from GO destroying MCF-7 cells *in vitro* and *in vivo*. Recently, Deng et al. developed a dual triggered hybrid microcapsule comprising GO, IONPs and polysaccharides *via* a layer-by-layer technique for on-demand drug release [101]. This nanosystem can release its payload by a dual-responsive trigger induced by both NIR and magnetic hyperthermia, making it highly controllable. The synergistic effect of hyperthermia (PTT and MHT) and chemotherapy successfully destroyed cervical cancer cells *in vitro* and *in vivo* (Fig. 9).

2.4. Electrically-triggered nanosystems for drug delivery

In the last years, electrically-triggered nanosystems (ETNs) have been developed as alternative remote-controlled delivery systems. The use of an electric field has several advantages for on-demand drug release, including reliability and precise control over the magnitude, duration, and intervals of pulses. Indeed, it offers the possibility to accurately regulate drug release levels [37,102,103]. Until now, a range of electrically-triggered nanosystems based on graphene (GETNs) including hydrogels have been designed for remote-controlled delivery. Most of GETNs consist of conductive polymers or conductive particles, which respond to an electric stimulus, and graphene, which not only improves the stability of the hydrogels, but also increases the drug loading. For example, Servant et al. prepared a graphene-based hydrogel as electroactive scaffold to control drug release (Fig. 10) [104]. The electroactive scaffold with enhanced mechanical, electrical, and thermal properties demonstrated controlled drug release upon the on/off application of a low direct current (DC) voltage (10 V) both in test tubes and *in vivo*.

Weaver et al. developed a delivery system by depositing GO inside a conducting polymer, polypyrrole (Ppy) [105]. The nanosystem was able to adsorb dexamethasone (an anti-inflammatory drug) and exhibited favorable electrical properties. Under electrical stimulation, the nanosystem released the drug *in vitro* with a linear profile and a dosage that could be controlled by altering the magnitude of the stimulation. More recently, Mac Kenna et al. developed an electroconductive hydrogel based on rGO for electrically-triggered drug release [106]. In this work, HA was used to improve the stability of the rGO dispersions. The rGO had the capacity to increase the mechanical strength and

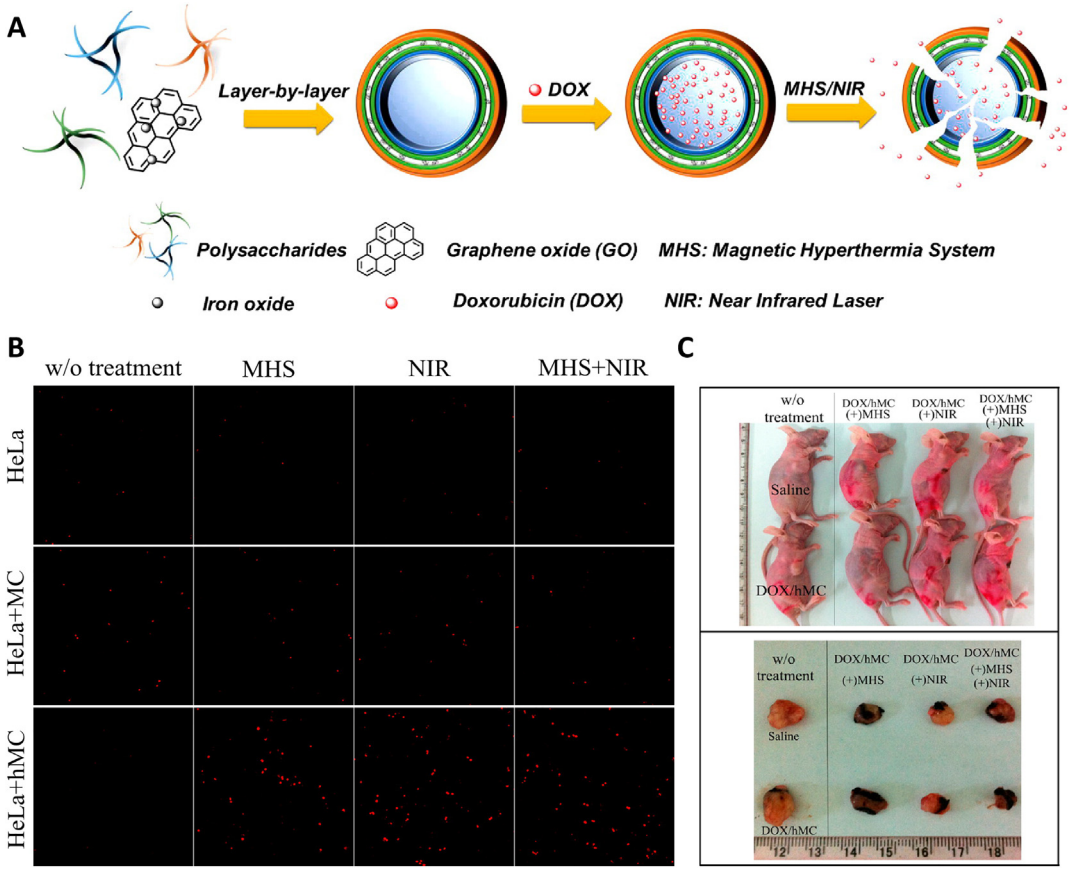

Fig. 9. (A) Schematic illustration of hybrid microcapsules (hMC) created *via* layer-by-layer assembly. (B) Confocal laser scanning microscopy images of dead cells incubated with different samples: control (without samples), microcapsules, and hybrid microcapsules. (C) *In vivo* study of hybrid microcapsules. Adapted from Deng et al. [101]. Copyright 2016 American Chemical Society.

electrochemical properties of the electroconductive hydrogel. This work showed that an electrical stimulation (− 0.6 V or + 0.6 V) could increase electrostatic repulsion between methyl orange (a model drug) and rGO to accelerate the drug release.

2.5. Multi-modal imaging nanosystems for therapy and diagnosis

Non-invasive tumor imaging is an important aspect throughout the entire process of cancer theranostics. Owing to large surface area, graphene can be easily modified with a range of molecules to prepare many multifunctional systems with outstanding performances, such as magnetism, fluorescence, radioactivity, plasmonic properties, *etc.* [24,41]. Multifunctional GO conjugates possess great potential in non-invasive imaging technology including MRI, positron emission tomography, X-ray computed tomography, fluorescence imaging, photoacoustic imaging (Fig. 11). In the last ten years, a series of multimodal imaging systems based on graphene have been explored to localize tumors, track cancer cells, follow drug delivery and monitor the cancer treatment in real time.

In 2012, Yang et al. developed IONP-modified PEG-rGO *via* a hydrothermal reaction [93]. After labeling with a radioactive or a fluorescent compound, this rGO derivative showed good ability for triple-modal fluorescence/MRI/PAI *in vivo* for 4T1 tumor imaging and imaging-guided PTT to destroy tumor cells (Fig. 11B). In another system, after grafting magnetic NPs and gold NPs on GO, the obtained conjugate (GO-IONP-Au) with both magnetic and plasmonic properties was successfully used for dual-modal magnetic resonance and X-ray imaging to monitor the efficiency of PTT (Fig. 11A) [95]. In the meantime, it was found that Ag NPs can also endow GO with plasmonic properties to achieve X-ray imaging-guided drug delivery and PTT to ablate breast tumor [73]. Chen et al. co-anchored Fe_3O_4 and manganese oxide on the surface of GO constructing a multiple stimuli-responsive nanosystem [107]. Upon triggering by acidic or into a redox environment, the manganese oxide significantly degraded into Mn^{2+} ions, leading to enhanced T_1-weighted and T_2-weighted MRI to monitor drug delivery. Recently, Song et al. developed a plasmonic gold nanorod hybridized rGO vesicle with amplified photoacoustic performance and photothermal effects (Fig. 11C) [74]. After labeling with the radioactive element ^{64}Cu, the multifunctional GO showed an excellent ability to localize tumor and allowed visualization of the shape and size of the tumor *via* PET and PAI.

3. Physically-triggered nanosystems based on 2D materials for therapy and diagnosis

Encouraged by the success and versatility of graphene within physically-triggered nanosystems, extensive efforts have equally contributed to the development of graphene-related materials (GRMs) for biomedical applications (Table 2). Due to the diversity of the constituent elements, 2D materials possess tunable optical, electrical, electrochemical, and thermal properties [19,108]. It is therefore possible to use external stimulations (laser, heat, electric field, magnetic field, ultrasound) to more precisely trigger therapeutic actions and to combine multiple diagnostic and therapeutic functions in a single 2D system. Until now, physically-triggered nanosystems based on GRMs have been widely explored for phototherapies, drug delivery, combination therapies and non-invasive imaging.

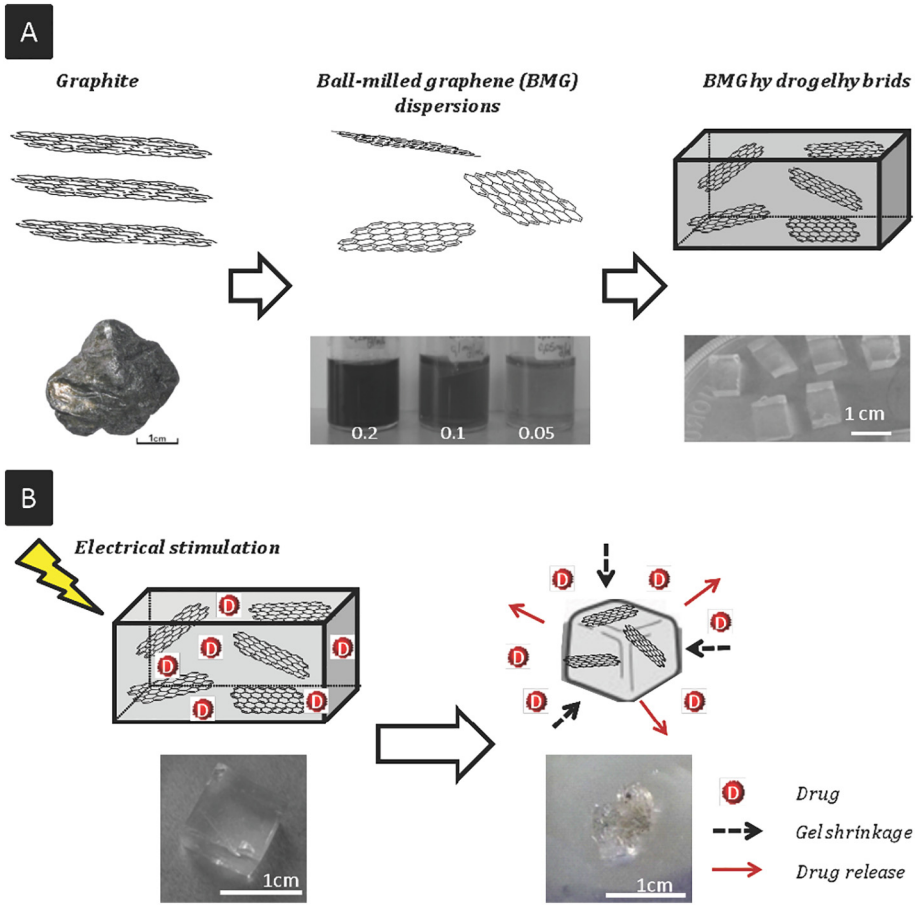

Fig. 10. Electroresponsive graphene/polymethylmethacrylic acid (PMAA) hydrogel hybrids for on-demand drug delivery. (A) The preparation process of graphene/hydrogel hybrid. (B) Drug release upon on/off application of a DC electric field and photos of the hydrogel before and after electrical stimulation. Reprinted from Servant et al. [104], Copyright 2014 WILEY-VCH Verlag GmbH & Co.

3.1. Light-triggered nanosystems based on 2D materials for therapy and diagnosis

3.1.1. Photothermal therapy using 2D materials

Considering the good NIR absorption capability, a range of 2D GRMs (*i.e.* MoS_2, WS_2, $MoSe_2$, TiS_2) with various surface modifications have been reported as photothermal agents to treat different types of cancer. MoS_2 nanosheets are well-known photothermal agents with strong absorption in the NIR spectral region. Their mass extinction coefficient is 29.2 $L \cdot g^{-1} \cdot cm^{-1}$ at 800 nm, even better than rGO (24.6 $L \cdot g^{-1} \cdot cm^{-1}$) and gold nanorods (13.9 $L \cdot g^{-1} \cdot cm^{-1}$) [109]. To overcome the poor dispersibility and colloidal stability in aqueous solutions, MoS_2 nanosheets were mainly modified by surface adsorption of polymers, such as chitosan, PEG, PEI, or soybean phospholipid [110]. Wang et al. synthesized a PEGylated MoS_2 that displayed an excellent colloidal and desired photothermal stability [111]. After intravenous administration, PEG-MoS_2 accumulated in the tumor *via* the EPR effect. Upon irradiation at 808 nm laser, the local generated heat caused the temperature increase of tumor tissues leading to ablation of 4T1 cancer cells. Recently, in order to enhance biocompatibility of MoS_2, Chen et al. developed a PEGylated MoS_2 (PEG-MoS_2) by a one-pot hydrothermal reaction in the presence of poly(acrylic acid) [112]. It was found that PEG-MoS_2 accumulated in tumor site and caused temperature increase up to 52.1 °C, significantly suppressing the growth of subcutaneously xenografted 4T1 tumor *in vivo* upon NIR irradiation. More importantly, this nanosheet degraded into water-soluble ions MoO_4^{2-} under physiological condition (pH = 7.4) with low adverse effect (Fig. 12).

Similar to MoS_2, WS_2 nanosheets also exhibit promising photothermal conversion capability for PTT. WS_2 nanosheets with a size of 50–100 nm were synthesized [113]. After PEGylation, the mass extinction coefficient of PEG-WS_2 at 808 nm was calculated to be 23.8 $L \cdot g^{-1} \cdot cm^{-1}$, which is similar to rGO. Following mice injection (either intratumorally or intravenously) of PEG-WS_2, the surface temperature of the tumor quickly raised to about 65 °C within 5 min by 808 nm irradiation at the laser power density of 0.8 $W \cdot cm^{-2}$. Liu et al. prepared WS_2 nanosheets intercalated with NH_4^+ *via* a bottom-up hydrothermal method [114]. These materials with a size of 150 nm possessed highly hydrophilic character and strong NIR absorption. Following the intratumor injection into tumor-bearing mice, the temperature of the tumor increased to 50 °C under NIR laser irradiation within 4 min leading to tumor disappearance after 4 days.

As another representative TMD material, molybdenum diselenide ($MoSe_2$) possesses a characteristic absorption peak located at ~ 800 nm, giving them a great potential as NIR photothermal transducers [115,116]. A number of reports have reported the utilization of $MoSe_2$-based nanomaterials as photothermal agents for PTT [117–120]. For example, Lei et al. modified $MoSe_2$ nanosheets with a biocompatible polymer PVP [117]. The resulting hydrophilic $MoSe_2$ nanosheets displayed good biocompatibility and a high photothermal conversion efficiency. Their mass extinction coefficient at 808 nm was calculated to be 11.1 $L \cdot g^{-1} \cdot cm^{-1}$, ~ 3-fold higher than that of GO nanosheets [3.6 $L \cdot g^{-1} \cdot cm^{-1}$] [109]. Under irradiation at 808 nm for 15 min, PVP-coated $MoSe_2$ nanosheets effectively killed HeLa cells at the concentration of 100 $\mu g \cdot mL^{-1}$. Furthermore, these $MoSe_2$ layers were successfully encapsulated into a thermoresponsive PNIPAM hydrogel matrix. This nanocomposite hydrogel exhibited a remote-controlled

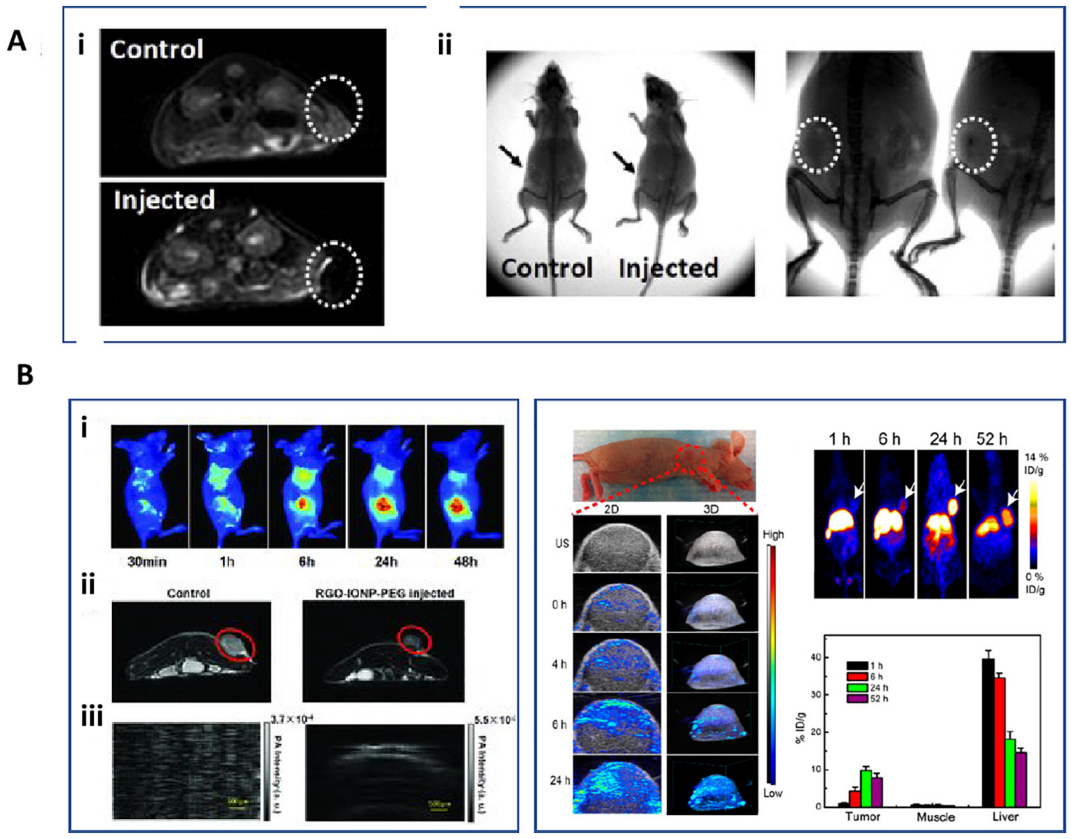

Fig. 11. (A) *In vivo* dual-modal MR/X-ray imaging of 4T1 tumor-bearing mice: (i) MRI, (ii) X-ray imaging. Adapted from Shi et al. [95]. Copyright 2013 Elsevier Ltd. (B) Multimodal imaging of 4T1 tumor-bearing mice after intravenous injection of rGO-IONP-PEG: (i) Fluorescence imaging using Cy5-labeled RGO-IONP-PEG; (ii) T_2-weighted MRI; and (iii) photoacoustic imaging. Adapted from Yang et al. [93]. Copyright 2012 WILEY-VCH Verlag GmbH & Co. (C) Dual-modal imaging of U87MG tumor *in vivo* after intravenous injection of rGO-loaded ultrasmall plasmonic gold nanorod vesicle (rGO-AuNRVe): (i) Ultrasound photoacoustic images; (ii) PET imaging; (iii) Biodistribution of rGO-AuNRVe in tumor, muscle, and liver at various time points. Adapted from Song et al. [74]. Copyright 2015 American Chemical Society.

photoresponsive capability for drug delivery and PTT towards cancer cells *in vitro*.

Bi_2Se_3 nanosheets have recently been demonstrated to be promising light-triggered nanosystem. In 2013, Li et al. found that Bi_2Se_3 nanoplates can absorb NIR laser light and effectively convert the laser energy into heat [121]. After modification with PVP, the Bi_2Se_3 nanosheets had good water dispersibility and biocompatibility. Under the irradiation of 808 nm laser, they successfully induced complete eradication of solid malignant tumors in mice. Recently, in order to improve tumor targeting and clearance of the nanosheets, Li et al. reported a strategy based on the transportation of Bi_2Se_3 nanosheets within macrophage vehicles for cell-mediated therapy [122]. Compared with bare Bi_2Se_3, the Bi_2Se_3-laden-macrophages, after intravenous injection, showed prolonged blood circulation and could overcome the hypoxia-associated drug delivery barrier to target the tumor efficiently and dramatically enhance the efficiency of photothermal cancer therapy.

As a new member of the 2D materials family, black phosphorus has received much interest for its unique 2D layered structure and layer-dependent bandgap of 0.3–2.0 eV. Because of its excellent optical properties such as strong NIR absorption and high photothermal conversion efficiency, BP has recently been adopted for PTT. Zhao et al. reported the functionalization of BP with Nile Blue (NB) dye *via* diazonium chemistry [123]. The resulting NB@BP displayed good biocompatibility and strong NIR fluorescence (680 nm). Under 808 nm NIR laser irradiation (1.0 $W \cdot cm^{-2}$) NB@BP exhibited excellent photothermal conversion ability, and the temperature increased by ~27.5 °C after 10 min. As a result of the stable NIR fluorescence and photothermal characteristics, the NB@BP were successfully used in both *in vivo* NIR fluorescence imaging and photothermal tumor ablation.

MXenes, another class of interesting 2D materials, owning the general formula of $M_{n+1}X_n$, where M is an early transition metal and X represents C and/or N (being $n = 1, 2,$ or 3) [124]. Due to their strong NIR absorption and high photothermal conversion efficiency, MXenes have attracted considerable attentions as PTT agents in biomedicine. Ti_3C_2 nanosheets showed a higher photothermal conversion efficient (30.6%) than Au nanorods (21%) [125]. After modifying Ti_3C_2 with soybean phospholipid (SP), the Ti_3C_2-SP complex could achieve a NIR light-induced tumor ablation without recurrence by either localized intratumoral injection or intravenous injection [126]. To endow MXenes with more functionalities to improve their theranostic applications, MnOx was grown on the surface of Ti_3C_2 to construct MnOx/Ti_3C_2 nanosheets for PAI/MRI-guided PTT [127]. In tumor microenvironment (mild acidic conditions), MnOx was degraded to Mn^{2+} to enhance T_1-weighted MRI for PTT guidance and monitoring. These nanosheets showed a high photothermal stability and a photothermal conversion efficiency of 22.9%. The MnOx/Ti_3C_2 nanosheets achieved a highly efficient tumor ablation and tumor-growth suppression (Fig. 13).

3.1.2. Photodynamic therapy using 2D materials

Similar to graphene, 2D GRMs can be loaded with PSs and used for remotely-triggered PDT for cancer treatment owing to their high surface area [128]. Moreover, due to their excellent photoelectric conversion performance, a range of GRMs have the inherent ability to produce ROS and can thus be used as PSs for PDT [129–133].

Graphitic-phase carbon nitride nanosheets, one of the newly emerging 2D layered nanomaterials, with high stability, good biocompatibility, low toxicity, and extremely high photoluminescence quantum yields can be obtained from direct sonication of bulk g-C_3N_4 in water.

Table 2
Physically-triggered nanosystems based on 2D materials for therapy and diagnosis.

2D material conjugates	Payloads	Physically trigger	Therapy	Imaging modes	*In vitro* models	*In vivo* models	Refs
PEG-WS_2	Gd^{3+}	Light	PTT/radiotherapy	PAI, CT, MRI	4T1 cells	Mice bearing 4T1 tumor	[29]
MoS_2-IONP-PEG	^{64}Cu	Light/magnetic	PTT	PET, PAI, MRI	4T1 cells	Mice bearing 4T1 tumor	[30]
MoS_2	/	Light	PTT	/	HeLa cells	/	[109]
MoS_2-soybean phospholipid	/	Light	PTT	/	4T1 cells	Mice bearing 4T1 tumor	[110]
PEG-MoS_2	/	Light	PTT	/	4T1 cells	Mice bearing 4T1 tumor	[111]
PEG-MoS_2	/	Light	PTT	/	4T1 cells	Mice bearing 4T1 tumor	[112]
PEG-WS_2	/	Light	PTT	CT, PAI	4T1 cells	Mice bearing 4T1 tumor	[113]
NH_4^+-WS_2	/	Light	PTT	/	HeLa cells	Mice bearing HeLa tumor	[114]
PVP-$MoSe_2$	DOX	Light	PTT/drug delivery	/	HeLa cells	/	[117]
PVP-Bi_2Se_3	/	Light	PTT	CT	H22 cells	Mice bearing H22 tumor	[121]
PVP-Bi_2Se_3	Macrophages	Light	PTT	/	RAW264.7 cells	Mice bearing MCF-7 tumor	[122]
NB-BP	/	Light	PTT	FI	MCF-7 cells	Mice bearing MCF-7 tumor	[123]
Ti_3C_2-SP	/	Light	PTT	/	4T1 cells	Mice bearing 4T1 tumor	[126]
MnO_x/Ti_3C_2—SP	/	Light	PTT	MRI, PAI	4T1 cells	Mice bearing 4T1 tumor	[127]
TPP-Fe^{III}-C_3N_4	MB	Light	PDT	MRI	HeLa cells	Mice bearing U14 tumor	[128]
g-C_3N_4	DOX	Light	PDT/drug delivery	/	HeLa cells	/	[129]
Black phosphorus	/	Light	PDT	/	MDA-MB-231 cells	Mice bearing MDA-MB-231 tumor	[130]
Galactose-MoS_2	/	Light	PDT	FI	HepG2 cells	/	[133]
PEG-MoS_2	DOX	Light	PTT/drug delivery	/	4T1 cells	Mice bearing 4T1 tumor	[135]
MoS_2-CS	DOX	Light	PTT/drug delivery	/	Panc-1 cells	Panc-1 tumor-bearing mice	[136]
PLGA/MoS_2	DOX	Light	PTT/drug delivery	/	4T1 cells	Mice bearing 4T1 tumor	[137]
WS_2-IO@MS-PEG	DOX	Light	PTT/drug delivery	FI, MRI, CT	4T1 cells	Mice bearing 4T1 tumor	[138]
MoS_2	siRNA	Light	PTT/gene silencing	/	4T1 cells	Mice bearing 4T1 tumor	[139]
PEI-WS_2	siRNA	Light	PTT/gene silencing	CT, PAI	BEL-7402 cells	Mice bearing BEL-7402 tumor	[140]
MoS_2-PEI-PEG	pDNA	Light/redox	PTT/gene delivery	/	HCT116 and B16F1 cells	/	[141]
BSA-WS_2	Methylene blue	Light	PTT/PDT	CT	HeLa cells	Mice bearing HeLa tumor	[142]
PEG-MoS_2	Ce6	Light	PTT/PDT	PAI	4T1 cells	Mice bearing 4T1 tumor	[143]
MoS_2-PEG-Au	Ce6	Light	PTT/PDT	CT, FI	4T1 cells	Mice bearing 4T1 tumor	[144]
PEG-MoS_2	Gd(III)	Magnetic	/	MRI	/	ICR mice	[145]
PEG-MoS_2-Fe_3O_4	/	Magnetic/light	PTT	MRI/PAI	HeLa and HepG2 cells	Mice bearing HeLa tumor	[146]
PEG-MoS_2-$Cu_{1.8}S$	DOX	Light	PTT/drug delivery	FI, PAI	A549 cells	Mice bearing A549 tumor	[148]

Lin et al. exploited g-C_3N_4 nanosheets for cancer imaging and therapy [129]. In this work, g-C_3N_4 nanosheets generated ROS, resulting in efficient cancer cell killing under low-intensity light irradiation (20 $mW \cdot cm^{-2}$). Moreover, similar to the loading and release properties of graphene, g-C_3N_4 nanosheets loaded with DOX showed pH-dependent drug delivery properties at acidic pH because of the increased protonation and solubility of DOX in the acidic environment. In addition, the water-dispersible g-C_3N_4 nanosheets with high photoluminescence quantum yields can be used for imaging. Another work has shown that Fe^{III}-modified g-C_3N_4 could react like peroxidase mimetics with excellent catalytic performance towards H_2O_2 for the generation of O_2 in cancer cells, thus overcoming tumor hypoxia and improving the PDT efficacy [128]. After covalent modification with (4-carboxybutyl)triphenylphosphonium (TPP) bromide, this mitochondria-targeting nanosystem had the ability to carry methylene blue (MB) as PS to mitochondria, leading to an almost complete destruction of mouse cervical tumor.

BP nanosheets can be used not only as photothermal agent due to their broad absorption range from UV and entire visible light region, but also as PSs due to their unique electronic structure. Wang et al. found that ultrathin BP nanosheets are efficient photosensitizers for the generation of singlet oxygen under visible light with a high $^1O_2$

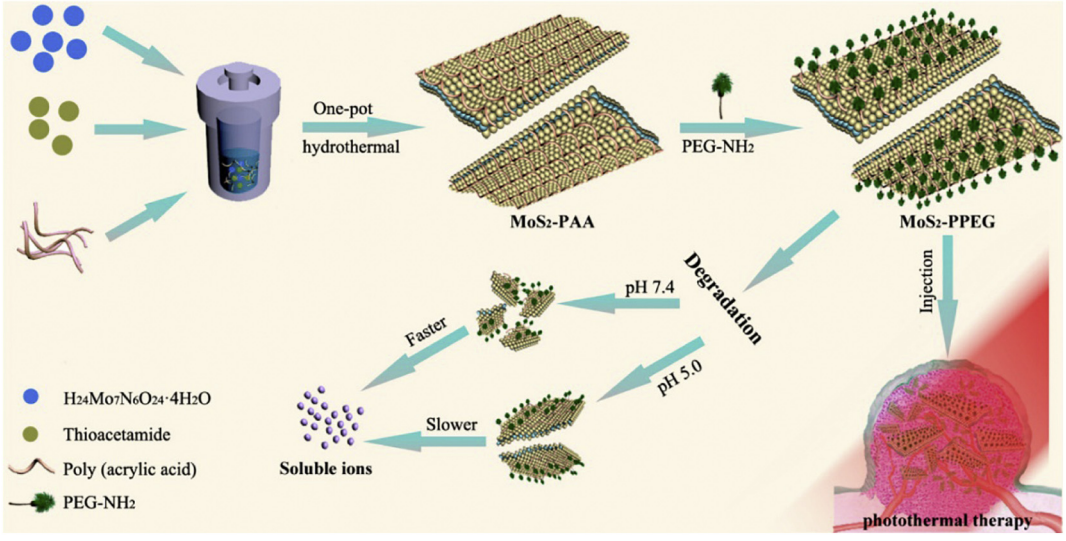

Fig. 12. Schematic diagram of preparation of PEG-MoS_2*via*a one-pot hydrothermal reaction. The obtained PEG-MoS_2 nanosheets showed good degradability in physiological environment (pH = 7.4) which can be used for *in vivo* photothermal cancer therapy. Reprinted from Chen et al. [112]. Copyright 2017 American Chemical Society.

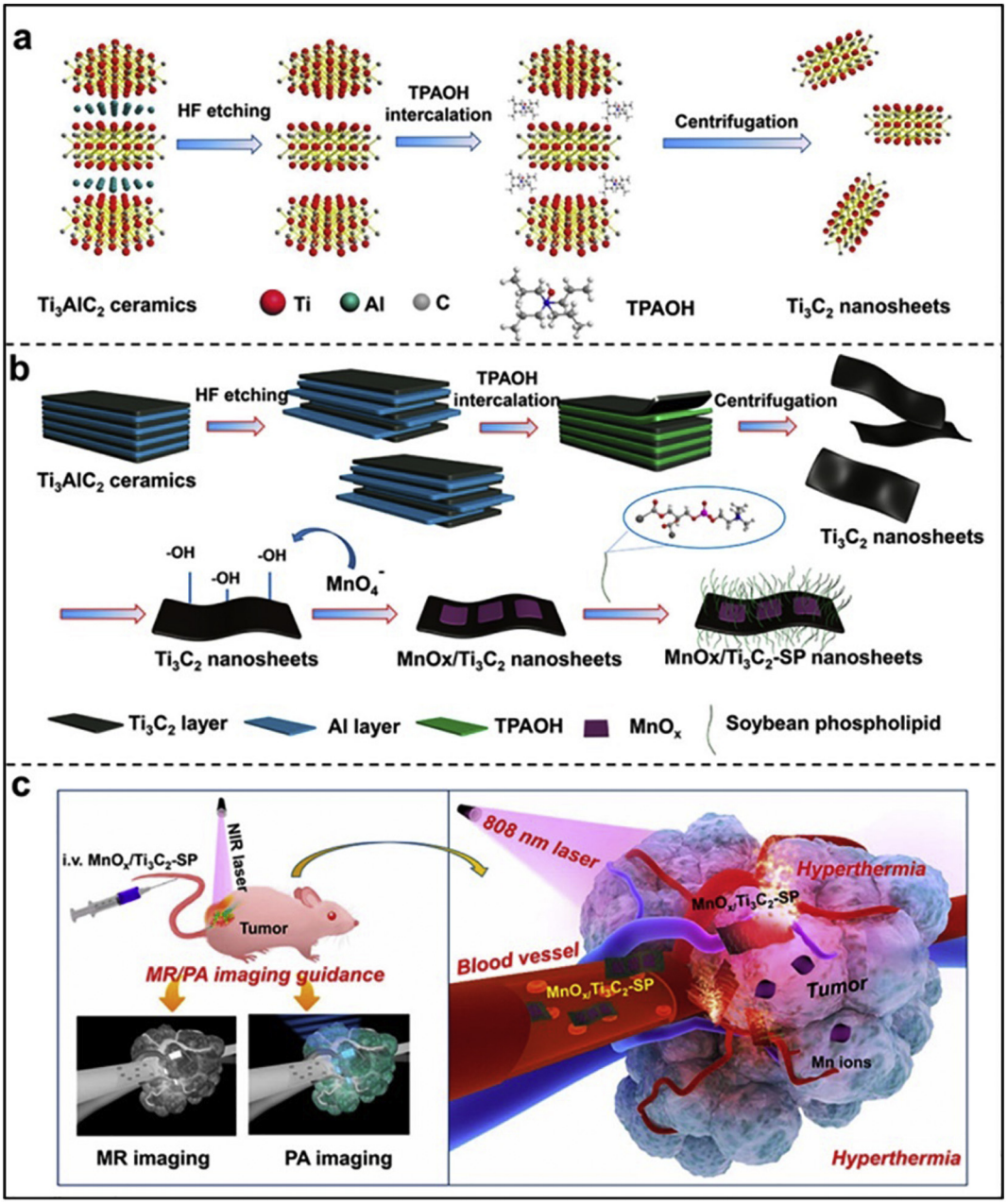

Fig. 13. Schematic illustration of the synthetic process and MRI/PAI-guided photothermal tumor therapy of MnOx/Ti_3C_2-SP nanosheets. (a) Scheme of the exfoliation process for 2D Ti_3C_2 nanosheets. (b) Scheme of the whole synthetic procedure for MnOx/Ti_3C_2-SP nanosheets. (c) Schematic illustration of theranostic functions of MnOx/Ti_3C_2-SP nanosheets, *i.e.*, MRI/PAI-guided efficient PTT ablation of cancer. Reprinted from Dai et al. [127]. Copyright 2017 American Chemical Society.

quantum yield (about 0.91) [130]. Under a short light irradiation time, a small amount of BP nanosheets exhibited a notable MDA-MB-231 breast tumor growth inhibition. Interestingly, the nanosheets were completely degraded into biocompatible phosphorus oxides under light irradiation, thus offering a great therapeutic potential for cancer treatment.

Glycoligand-protein interactions are pivotal biological events that are also involved in human diseases such as cancer, influenza, and inflammation [134]. Ji et al. have developed MoS_2 glycosheets by the supramolecular self-assembly of fluorophore-labeled glycoligands on MoS_2 [133]. Due to the specific glycoligand-receptor recognitions, the galactose-modified MoS_2 sheets could be selectively internalized into the HepG2 cells that highly express the galactose receptors. They showed a good ability to produce ROS under visible light irradiation leading to apoptosis of the cancer cells (Fig. 14).

3.1.3. Combined photothermal therapy and drug/gene delivery

Due to the high surface-to-volume ratio and ultrahigh surface area, 2D GRMs are regarded as ideal carriers with high drug loading capacity. Indeed, GRMs have been demonstrated as efficient carriers for drugs and genes [27,63]. In addition, the unique chemical composition of GRMs can induce specific interactions with drug molecules allowing external triggers for on-demand drug release. Moreover, owing to their outstanding photothermal conversion properties, multifunctional GRMs can achieve a synergistically therapeutic outcome, such as combination of PTT and chemotherapy or gene therapy.

For example, Liu et al. found that PEGylated MoS_2 with high photothermal conversion efficiency displayed high loading values for three anticancer drugs (~39 wt% for Ce6, ~118 wt% for SN38, ~239 wt% for DOX) [135]. Using a low dose of DOX-loaded PEG-MoS_2 nanosheets, the combined PTT/chemotherapy achieved synergistic anticancer effect

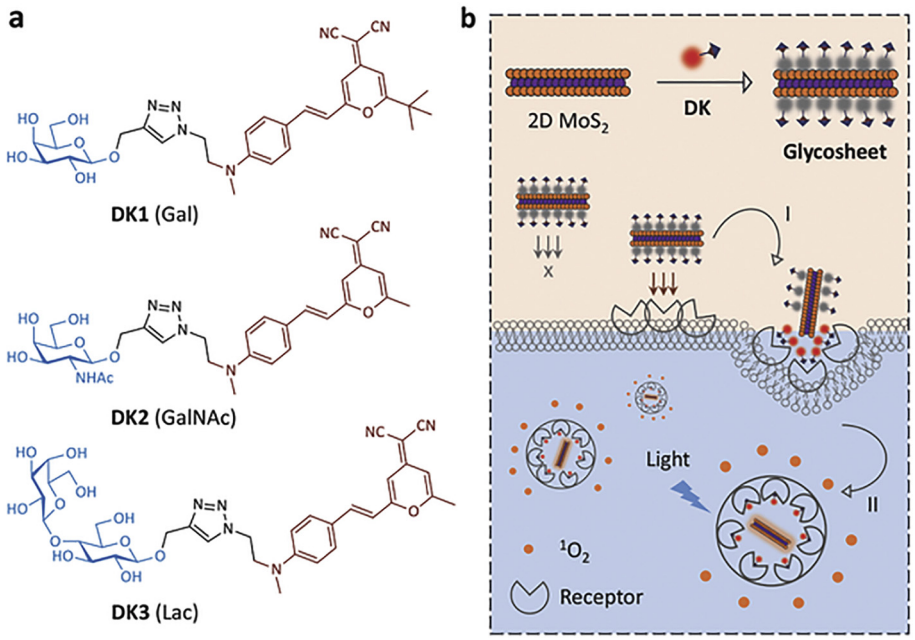

Fig. 14. (a) Structures of the dicyanomethylene-4*H*-pyran-tagged glycoligands DK1, DK2, and DK3 (Gal = galactose; GalNAc = *N*-acetyl galactosamine; Lac = lactose). (b) Schematic illustration of the supramolecular self-assembly between 2D MoS_2 and DK glycoligand to form the glycosheet, and their targeted intracellular production of singlet oxygen through two stages: (i) the receptor-mediated endocytosis, and (ii) the light irradiation. Adapted from Ji et al. [133]. Copyright 2016 WILEY-VCH Verlag GmbH & Co.

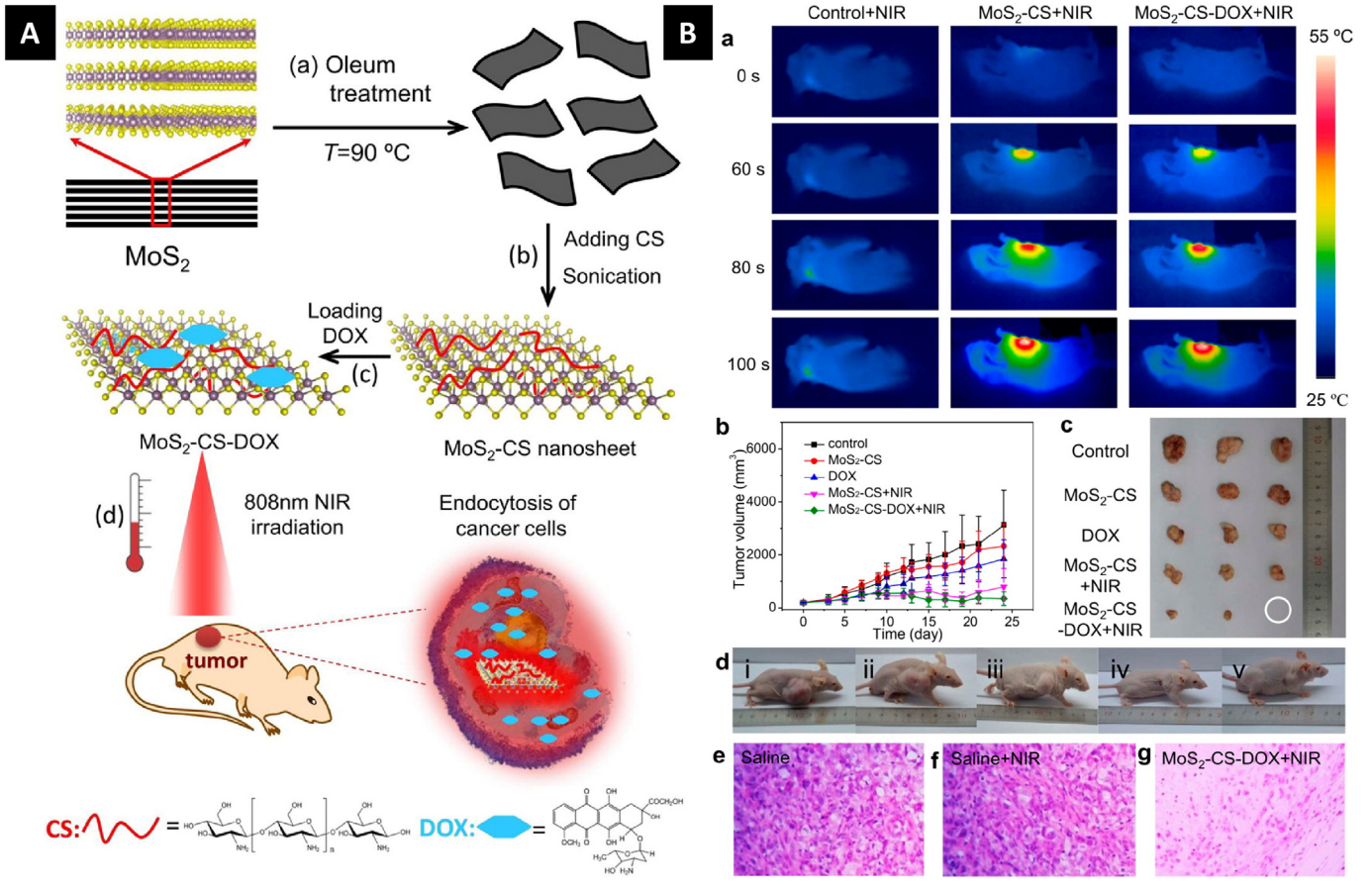

Fig. 15. (A) Schematic illustration of the high-throughput synthesis of MoS_2-CS nanosheets as NIR photothermal-triggered drug delivery systems for efficient cancer therapy. (B) Comparative investigation of inhibiting tumor effectiveness *in vivo*. (a) Infrared thermal images of Panc-1 tumor-bearing mice injected with saline, MoS_2-CS + NIR laser, and MoS_2-CS-DOX + NIR. (b) Tumor growth curves after various treatments (five groups). (c) Photograph of tumors from the control group, MoS_2-CS group, DOX group, MoS_2-CS + NIR group, and MoS_2-CS-DOX + NIR group. (d) Photographs of the typical mice of tested groups corresponding to saline+NIR (i), MoS_2-CS (ii), DOX (iii), MoS_2-CS + NIR (iv), and MoS_2-CS-DOX (v) after observation for 24 days. (e-g) Histological images of tumors collected from the groups of saline (e), saline+NIR (f), and MoS_2-CS-DOX + NIR (g). Adapted from Yin et al. [136] Copyright 2014 American Chemical Society.

in inhibiting 4T1 tumor growth under 808 nm laser irradiation. Yin et al. explored chitosan (CS)-modified MoS_2 nanosheets with high NIR absorption and high photothermal conversion efficiency (24.4%) [136]. DOX was loaded onto MoS_2-CS and it was found that NIR light-induced local hyperthermia induced the release of DOX from MoS_2-CS, resulting in enhanced antitumor efficacy for the treatment of pancreatic cancer (Fig. 15).

Alternatively, Wang et al. encapsulated MoS_2 nanosheets and DOX in a poly(lactic-*co*-glycolic acid) (PLGA) based implant matrix for *in vivo* use [137]. Upon NIR laser irradiation, the generated heat not only caused significant tumor necrosis but also enhanced the tumor chemotherapeutic efficiency by triggering fast release of encapsulated DOX molecules. 4T1 tumor could be completely erased without recurrence. Similarly, 2D WS_2 also showed the ability for combined PTT and drug delivery. Yang et al. loaded IONPs and mesoporous silica shells onto PEG-WS_2 (WS_2-IO@MS-PEG) [138]. The multifunctional WS_2 exhibited high NIR and X-ray absorbance, as well as strong superparamagnetic properties. Combined PTT/chemotherapy was then carried out *in vivo* using WS_2-IO@MS-PEG/DOX, achieving a remarkably synergistic therapeutic effect superior to the respective mono-therapies.

Recently, light-triggered gene delivery based on GRMs has attracted increasing attention to remove some obstacles in cellular gene delivery such as low uptake by cells and undesired release efficiency of payloads at targeting site [139]. Because of the depth-dependent decrease of laser intensity, a high-power laser is generally required to eradicate tumor by PTT. The high temperature may cause unavoidable collateral damage to normal tissue and exceed the tolerance of patients. To address this problem, Zhang et al. used PEI-WS_2-siRNA as platform for gene-photothermal synergistic therapy of tumors in mild conditions [140]. As a member of the family of apoptosis inhibitors, survivin siRNA could inhibit heat shock response and thus makes cancer cells more sensitive to heat at mild temperature. A high inhibition of liver tumor (91.7%) without recurrence was observed after combined PTT/gene silencing. In order to increase gene delivery efficiency, Kim et al. immobilized PEI and PEG on MoS_2 (MoS_2-PEI-PEG), which is sensitive to both external (light) and internal stimuli (glutathione, GSH), achieving efficient gene delivery by a step-by-step approach [141]. The MoS_2-PEI-PEG carrying plasmid DNA (pDNA) entered into human colon cancer cells (HCT116) by endocytosis. When the nanosystem was trapped inside the endosomes, NIR laser was used to generate local heat that resulted in endosomal membrane rupture, inducing endosomal escape of MoS_2-PEI-PEG-pDNA. After endosomal escape, the polymers were detached from MoS_2 by GSH, resulting in effective gene release from the nanosheets. The transfection efficiency of MoS_2-PEI-PEG increased by ~2.5 times in HCT116 cells and by ~4 times in B16F1 cells upon 808 nm laser irradiation (Fig. 16).

3.1.4. Combined photodynamic and photothermal therapy

Photosensitizers, light and oxygen are the three key components for generation of $^1O_2$ in PDT [46]. However, the hypoxic microenvironments of tumors usually lead to low generation of $^1O_2$, which limits its therapeutic efficacy. To solve this problem, PTT has been used to

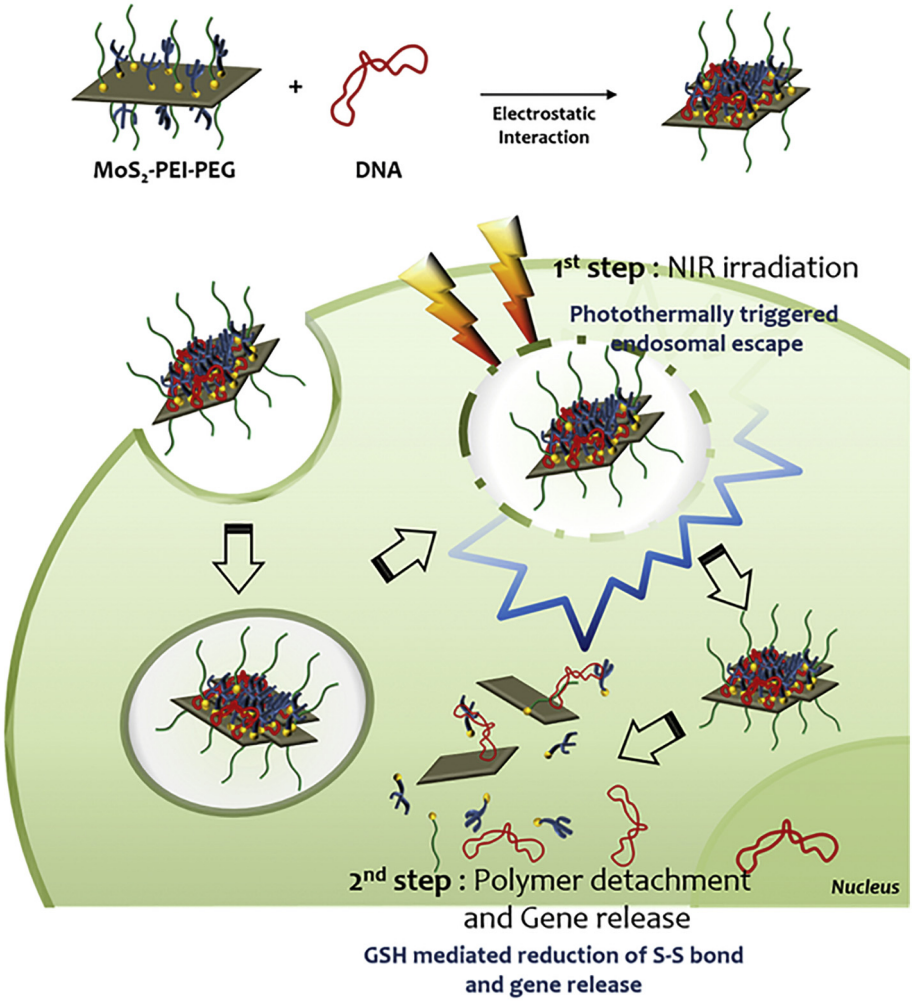

Fig. 16. Schematic illustration of sequential pDNA delivery using MoS_2-PEI-PEG by photothermally triggered endosomal escape followed by redox-mediated polymer detachment and DNA release. Adapted from Kim et al. [141]. Copyright from 2016 Wiley-VCH Verlag GmbH & Co.

improve PDT efficiency. Mild hyperthermia not only increases the cellular uptake of PSs, but it also increases intratumoral blood flow which further transports more oxygen into the cancer cells [26]. Combination of PTT and PDT has been demonstrated being a highly efficient approach for cancer therapy.

Yong et al. employed WS_2 nanosheets functionalized with bovine serum albumin (BSA) as drug carriers to adsorb the PS MB for combined PTT and PDT treatment of cancer cells [142]. Due to the effective energy transfer between MB and WS_2, singlet-oxygen generation by MB was efficiently inhibited by the WS_2 nanosheets. Under NIR irradiation (808 nm), the local heat generated by BSA-WS_2 not only killed cancer cells, but also triggered MB release resulting in the efficient restoration of singlet-oxygen generation for PDT application. The *in vitro* results showed that the efficacy of the combined PDT/PTT treatment of cancer cells was higher than that of PDT and PTT alone. Furthermore, Liu et al. first applied PDT/PTT combined therapy in animal experiments [143]. In this work, PEGylated MoS_2 nanosheets were exploited as drug carrier of Ce6. Under 808 nm laser irradiation, mild heating increased cell membrane permeability and promoted cellular uptake, inducing enhanced intracellular delivery of Ce6. The nanosheets significantly killed cancer cells upon exposure to 808 nm laser irradiation (PTT) and 660 nm (PDT), achieving synergistic effect in delaying 4T1 breast tumor growth. Another report showed that PEG-MoS_2 decorated with Au NPs (MoS_2-PEG-Au) displayed enhanced photothermal conversion efficiency compared to PEG-MoS_2 and a Ce6 loading capacity of 23.1 wt% [144]. Upon 808 nm laser irradiation, over 45% of Ce6 was released from MoS_2 surface. *In vivo* experiments using two lasers (660 nm and 808 nm) showed that PTT (808 nm) remotely induced Ce6 release and ROS generation (660 nm), thus achieving synergistic effect of PTT and PDT for antitumor therapy.

3.2. Magnetic-triggered nanosystems for therapy and diagnosis

Similar to graphene, a range of 2D GRMs have been explored for MRI and magnetic-triggered drug delivery after coating with IONPs or gadolinium complexes. For example, Anbazhagan et al. developed a core-shell magnetic hybrid made of MoS_2 and gadolinium [145]. This system exhibited enhanced paramagnetic properties with 4.5 times longer water proton spin-lattice relaxation time when compared to commercial gadolinium CAs. MRI revealed a hyperintense signal *in vivo* and showed that it was easily cleared from the body. In another work [138], WS_2 nanosheets were pre-adsorbed with IONPs, and after coating with PEGylated mesoporous silica shell (MS), the obtained WS_2-IO@MS-PEG displayed strong superparamagnetic properties and high NIR absorbance, and it was used for T_2-weighted MRI. Yu et al. explored magnetic targeted PTT by the combination of MoS_2 flakes and Fe_3O_4 NPs [146]. In this work, MoS_2-Fe_3O_4 could be moved and hijacked to tumor site under external magnetic field. This smart nanosystem not only showed an enhanced photothermal ablation of cancer cells *in vivo* upon exposure to 808 nm NIR laser, but it also showed the ability to be used as T_2-weighted MRI CA.

3.3. Multi-modal nanosystems for therapy and diagnosis

Up to now, a range of multimodal GRMs have been used to offer better accuracy for cancer diagnosis and therapy. Due to their large surface area, 2D graphene-like materials can adsorb different types of imaging molecules and nanoparticles such as fluorophores, Gd, radioactive elements, IONPs and other NPs, to allow them to be used for many non-invasive imaging modalities including MRI, FI, and CT. In addition, due to the diversity of elemental composition, the intrinsic properties of GRMs can be exploited for multimodal imaging. For example, both MoS_2 and WS_2 nanosheets possess strong X-ray attenuation ability. They have been used as X-ray CAs for CT imaging, leading to enhanced contrast images compared to some commercial CAs [113,136]. Due to their strong NIR absorption, GRMs (such as MoS_2, TiS_2 [147]) can also generate ultrasound signal for PAI.

In 2014, Cheng et al. found that PEG-modified WS_2 nanosheets possessed strong X-ray attenuation ability and high NIR absorbance [113]. Its Hounsfield units (HU) value (about 22.01 HU $L \cdot g^{-1}$) was higher than commercial CT CA iopromide (15.9 HU $L \cdot g^{-1}$). After either i.t. or i.v. injection, the PEG-WS_2 nanosheets served as CAs for CT and PAI to monitor PTT of 4T1 tumor. Furthermore, Gd^{3+} has been grown onto PEG-WS_2 to endow WS_2 with strong contrast in T_1-weighted MRI for allowing triple-modal CT/MRI/PAI and imaging-guided PTT and radiotherapy [29]. In this multimodal nanosystem, the two-dimensional transition metal dichalcogenide intrinsic properties enabled PAI and PTT, while both W and Gd elements attenuated X-ray irradiation to enable CT imaging and enhanced radiotherapy (Fig. 17).

Liu et al. prepared multifunctional theranostic nanosheets based on MoS_2 for multimodal imaging-guided cancer therapy [30]. In this work, MoS_2 nanosheets were functionalized with IONPs and positron-emitting radioisotope ^{64}Cu without using a chelating agent for PET, PAI and MRI. Under the guidance of the triple imaging modalities, *in vivo* PTT using MoS_2-IONP-PEG achieved effective tumor ablation in 4T1 animal tumor model.

Very recently, Meng et al. decorated MoS_2 with $Cu_{1.8}S$ NPs *via in situ* growth [148]. After conjugating MoS_2/$Cu_{1.8}S$ with a targeting aptamer and PEG, multifunctional MoS_2 hybrid nanosheets with a high photothermal conversion efficiency (32.5%) were obtained. The fluorescent MoS_2 and $Cu_{1.8}S$ NPs allowed photoluminescence imaging and PAI, respectively, as well as photothermal imaging for multimodality imaging diagnosis of cancer. In addition, it enabled to target A549 cells specifically and deliver molecular beacon probe with the miRNA-155 to detect intracellular microRNA and DOX for chemotherapy under NIR irradiation. This targeted chemo-photothermal therapy presented excellent *in vitro* and *in vivo* antitumor efficiency.

4. Conclusion and perspectives

In summary, we have reviewed the recent developments of physically-triggered nanosystems based on 2D materials from design to biomedical applications. The physical triggers mainly include light, heat, magnetic and electric field. These systems with unique properties provide various innovative methods for cancer theranostics, including phototherapies, magnetic therapy, remotely controlled chemotherapy, and non-invasive imaging. Although tremendous efforts have been made to improve the performance of physically-triggered nanosystems, to date no such systems have been utilized in clinic. The physically-triggered theranostics based on 2D materials is still in its early stage of development and requires considerable efforts on several aspects listed below:

1. *Biocompatibility of 2D materials*. The biocompatibility is one of the primary challenges to exploit 2D nanomaterials for biomedical applications. To date, there is a huge amount of studies on graphene-family nanomaterials (but it is difficult to generalize) and much less on newly emerged other 2D materials. There has been a wide consensus that 2D materials can pose potential risks to living organisms due to their toxicity to various living organisms and cells [149–151]. Many efforts have been made to study their toxicity mechanism and try to alleviate their toxicity. Some studies have shown that functionalized graphene and 2D materials do not produce any cytotoxic effect and do not cause immune response [152–154]. Simultaneously, some studies have demonstrated that graphene can be degraded by human myeloperoxidase in the presence of hydrogen peroxide [155] and signs of *in vivo* degradation have been evidenced [156]. Furthermore, some functionalized 2D materials, such as MoS_2 [112,157], MnO_2 [158,159], BP [130,160] can be degraded in physiological environments and transformed into ions, which can be easily eliminated from the body. However,

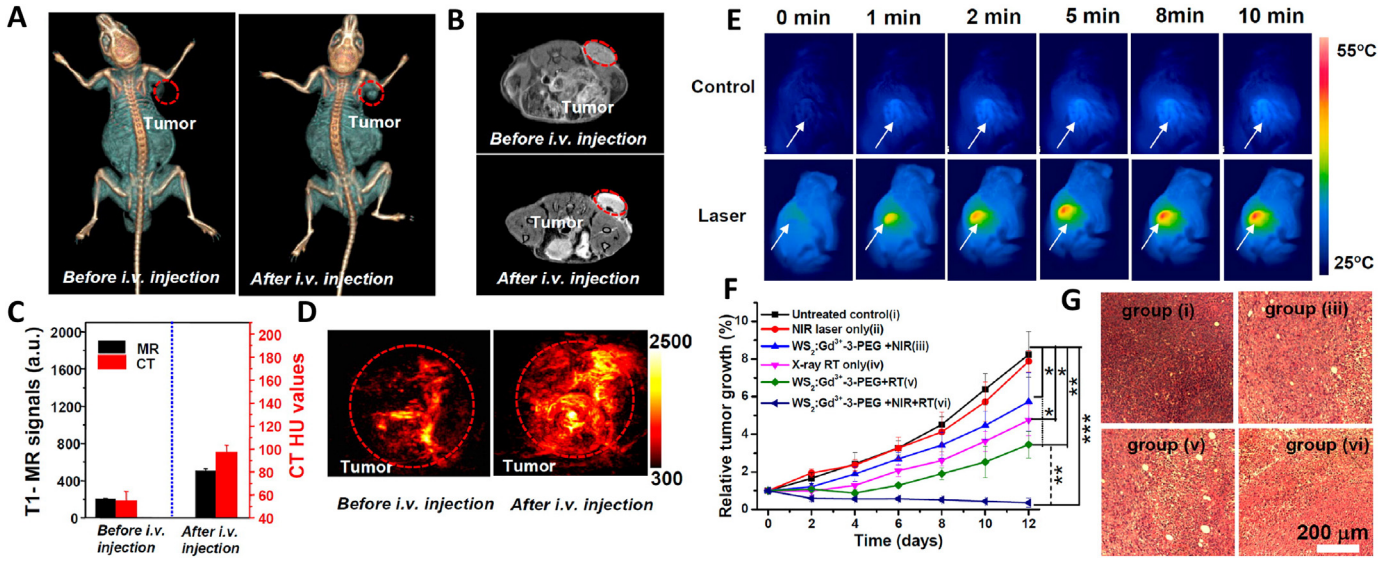

Fig. 17. *In vivo* triple-modal imaging in 4T1 tumor-bearing mice before and 24 h after i.v. injection of PEG-WS_2:Gd^{3+} and combined PTT and radiotherapy. (A) *In vivo* CT images of mice. (B) T_1-weighted MR images of mice. (C) Quantified MR and CT signals of tumors from mice based on images in (A) and (B). (D) *In vivo* PA images of tumors in mice. (E) IR thermal images of mice without or with i.v. injection of PEG-WS_2/Gd^{3+} under 808 nm laser irradiation taken at different time intervals. (F) Tumor volume growth curves of mice after various treatments. (G) Micrographs of H&E-stained tumor slices. Adapted from Cheng et al. [29] Copyright 2015 American Chemical Society.

the long-term toxicology evaluation *in vivo* is still needed to demonstrate the safety of 2D material-based nanomedicines for further use in clinic.

2. *Standardization of 2D materials*. It is widely accepted that the size, shape, and surface modification of 2D materials have an important influence on their toxicology and performances, as well as they critically impact their fate in physiological environments [150,161,162]. However, it is difficult to precisely control the size and shape of 2D materials with current preparation technology. 2D materials obtained by similar methods can even possess large size span and structural differences. This lack of control makes the systematic evaluation of their biological interactions challenging. Therefore, there is immense interest in preparing 2D nanomaterials with uniform size and shape by innovative preparation technology.
3. *The diversity of 2D materials*. Since isolation of graphene in 2004, about 30 different 2D materials with unique properties have been explored and utilized as physically-triggered nanosystems. It is only a drop in the ocean compared with the huge number of 2D materials. Therefore, 2D materials, which may have novel properties for biomedical applications definitely need investigation.
4. *Working modes of nanosystems*. Physically-triggered nanosystems should be controlled by efficient stimuli to adapt to our demand. However, due to the complexity of physiological environment, it is unavoidable that they can be disturbed by extensive interference factors. In addition, each physical trigger has its own limitations. For example, shallow tissue penetration is an issue for light-triggered phototherapy, especially PTT, whereas magnetic therapies usually need a high dose of magnetic NPs to be efficient. By integrating the advantages of each physical trigger, developing multimodal physically-triggered nanosystems will allow overcoming these limitations.
5. *Potential applications of nanosystems in immunotherapy*. As mentioned above, with a deep insight of intrinsic characteristic of 2D materials, different anti-tumor applications of physically-triggered nanosystems have been constantly discovered. However, there is still much room to further find new biomedical applications of physically-triggered nanosystems to improve the cure rates for the treatment of tumors. Recently, cancer immunotherapy based on nanomaterials is attracting growing attention. Indeed, it was found that phototherapy using nanomaterials can trigger anti-tumor immune response to efficiently inhibit tumor metastasis bringing a significant improvement of cure rates [163], giving new horizons in immunotherapy and vaccine development [164,165]. Encouraged by this discovery, other nanosystems have been developed for treating tumor metastasis by combined PTT and immunotherapy [166–168]. Considering the unique photothermal and photodynamic features of 2D materials, in our opinion, cancer immunotherapy of physically-triggered nanosystems based on 2D materials could be a new direction for cancer treatment.

An ideal "smart" nanosystem should be like a nanorobot that can automatically identify a disease and not release its payloads until triggered by stimuli at the target site, thus destroying targeting cells and not normal cells and tissues. In addition, its residence time, working position *in vivo* should be precisely controlled in real time. There is no doubt that it is not easy to achieve these objectives, but we do believe that it is just a matter of time before getting the perfect nanosystem with unremitting joint efforts of material scientists, chemists, physicists, biologists, and medical doctors.

Acknowledgments

This work was supported by the Centre National de la Recherche Scientique (CNRS), by the Agence Nationale de la Recherche (ANR) through the LabEx project Chemistry of Complex Systems (ANR-10-LABX-0026_CSC) (to A.B.), and by the International Center for Frontier Research in Chemistry (icFRC). The authors gratefully acknowledge financial support from ANR (ANR-15-GRFL-0001-05) (G-IMMUNOMICS project).

References

[1] J.T. Santini, M.J. Cima, R. Langer, A controlled-release microchip, Nature 397 (1999) 335–338.
[2] S. Mura, J. Nicolas, P. Couvreur, Stimuli-responsive nanocarriers for drug delivery, Nat. Mater. 12 (2013) 991–1003.
[3] M. van Elk, B.P. Murphy, T. Eufrásio-Da-Silva, D.P. O'Reilly, T. Vermonden, W.E. Hennink, G.P. Duffy, E. Ruiz-Hernández, Nanomedicines for advanced cancer treatments: transitioning towards responsive systems, Int. J. Pharm. 515 (2016) 132–164.
[4] D. Liu, F. Yang, F. Xiong, N. Gu, The smart drug delivery system and its clinical potential, Theranostics. 6 (2016) 1306–1323.
[5] C. Ding, L. Tong, J. Feng, J. Fu, Recent advances in stimuli-responsive release function drug delivery systems for tumor treatment, Molecules 21 (2016) 1715.

[6] M.A.C. Stuart, W.T.S. Huck, J. Genzer, M. Müller, C. Ober, M. Stamm, G.B. Sukhorukov, I. Szleifer, V.V. Tsukruk, M. Urban, F. Winnik, S. Zauscher, I. Luzinov, S. Minko, Emerging applications of stimuli-responsive polymer materials, Nat. Mater. 9 (2010) 101–113.

[7] M. Liu, H. Du, W. Zhang, G. Zhai, Internal stimuli-responsive nanocarriers for drug delivery: design strategies and applications, Mater. Sci. Eng. C. 71 (2017) 1267–1280.

[8] J. Yu, X. Chu, Y. Hou, Stimuli-responsive cancer therapy based on nanoparticles, Chem. Commun. 50 (2014) 11614–11630.

[9] B. Taghizadeh, S. Taranejoo, S.A. Monemian, Z. Salehi Moghaddam, K. Daliri, H. Derakhshankhah, Z. Derakhshani, Classification of stimuli–responsive polymers as anticancer drug delivery systems, Drug Deliv. 22 (2015) 145–155.

[10] N. Kamaly, B. Yameen, J. Wu, O.C. Farokhzad, Degradable controlled-release polymers and polymeric nanoparticles: mechanisms of controlling drug release, Chem. Rev. 116 (2016) 2602–2663.

[11] K. Yang, L. Feng, Z. Liu, Stimuli responsive drug delivery systems based on nano-graphene for cancer therapy, Adv. Drug Deliv. Rev. 105 (2016) 228–241.

[12] V. Georgakilas, J.N. Tiwari, K.C. Kemp, J.A. Perman, A.B. Bourlinos, K.S. Kim, R. Zboril, Noncovalent functionalization of graphene and graphene oxide for energy materials, biosensing, catalytic, and biomedical applications, Chem. Rev. 116 (2016) 5464–5519.

[13] S. Augustine, J. Singh, M. Srivastava, M. Sharma, A. Das, B.D. Malhotra, Recent advances in carbon based nanosystems for cancer theranostics, Biomater. Sci. 5 (2017) 901–952.

[14] J. Yao, J. Feng, J. Chen, External-stimuli responsive systems for cancer theranostic, Asian J. Pharm. Sci. 11 (2016) 585–595.

[15] R. Ahmad, Z. Ali, X. Mou, J. Wang, H. Yi, N. He, Recent advances in magnetic nanoparticle design for cancer therapy, J. Nanosci. Nanotechnol. 16 (2016) 9393–9403.

[16] K.S. Novoselov, Electric field effect in atomically thin carbon films, Science 306 (2004) 666–669.

[17] D. Chimene, D.L. Alge, A.K. Gaharwar, Two-dimensional nanomaterials for biomedical applications: emerging trends and future prospects, Adv. Mater. 27 (2015) 7261–7284.

[18] G.R. Bhimanapati, Z. Lin, V. Meunier, Y. Jung, J. Cha, S. Das, D. Xiao, Y. Son, M.S. Strano, V.R. Cooper, L. Liang, S.G. Louie, E. Ringe, W. Zhou, S.S. Kim, R.R. Naik, B.G. Sumpter, H. Terrones, F. Xia, Y. Wang, J. Zhu, D. Akinwande, N. Alem, J.A. Schuller, R.E. Schaak, M. Terrones, J.A. Robinson, Recent advances in two-dimensional materials beyond graphene, ACS Nano 9 (2015) 11509–11539.

[19] K.J. Koski, Y. Cui, The new skinny in two-dimensional nanomaterials, ACS Nano 7 (2013) 3739–3743.

[20] Z. Wang, W. Zhu, Y. Qiu, X. Yi, A. von dem Bussche, A. Kane, H. Gao, K. Koski, R. Hurt, Biological and environmental interactions of emerging two-dimensional nanomaterials, Chem. Soc. Rev. 45 (2016) 1750–1780.

[21] R. Kurapati, K. Kostarelos, M. Prato, A. Bianco, Biomedical uses for 2D materials beyond graphene: current advances and challenges ahead, Adv. Mater. 28 (2016) 6052–6074.

[22] L. Mo, J. Li, Q. Liu, L. Qiu, W. Tan, Nucleic acid-functionalized transition metal nanosheets for biosensing applications, Biosens. Bioelectron. 89 (2017) 201–211.

[23] X. Li, J. Shan, W. Zhang, S. Su, L. Yuwen, L. Wang, Recent advances in synthesis and biomedical applications of two-dimensional transition metal dichalcogenide nanosheets, Small 13 (2017), 1602660. .

[24] Y. Zhou, X. Jing, Y. Chen, Material chemistry of graphene oxide-based nanocomposites for theranostic nanomedicine, J. Mater. Chem. B 5 (2017) 6451–6470.

[25] X.-P. He, H. Tian, Photoluminescence architectures for disease diagnosis: from graphene to thin-layer transition metal dichalcogenides and oxides, Small 12 (2016) 144–160.

[26] L. Gong, L. Yan, R. Zhou, J. Xie, W. Wu, Z. Gu, Two-dimensional transition metal dichalcogenide nanomaterials for combination cancer therapy, J. Mater. Chem. B 5 (2017) 1873–1895.

[27] Y. Chen, Y. Wu, B. Sun, S. Liu, H. Liu, Two-dimensional nanomaterials for cancer nanotheranostics, Small 13 (2017), 1603446. .

[28] Y. Chen, C. Tan, H. Zhang, L. Wang, Two-dimensional graphene analogues for biomedical applications, Chem. Soc. Rev. 44 (2015) 2681–2701.

[29] L. Cheng, C. Yuan, S. Shen, X. Yi, H. Gong, K. Yang, Z. Liu, Bottom-up synthesis of metal-ion-doped WS_2 nanoflakes for cancer theranostics, ACS Nano 9 (2015) 11090–11101.

[30] T. Liu, S. Shi, C. Liang, S. Shen, L. Cheng, C. Wang, X. Song, S. Goel, T.E. Barnhart, W. Cai, Z. Liu, Iron oxide decorated MoS_2 nanosheets with double PEGylation for chelator-free radiolabeling and multimodal imaging guided photothermal therapy, ACS Nano 9 (2015) 950–960.

[31] F. Tian, J. Lyu, J. Shi, M. Yang, Graphene and graphene-like two-denominational materials based fluorescence resonance energy transfer (FRET) assays for biological applications, Biosens. Bioelectron. 89 (2017) 123–135.

[32] J. Li, F. Cheng, H. Huang, L. Li, J.-J. Zhu, Nanomaterial-based activatable imaging probes: from design to biological applications, Chem. Soc. Rev. 44 (2015) 7855–7880.

[33] J. Liu, L. Cui, D. Losic, Graphene and graphene oxide as new nanocarriers for drug delivery applications, Acta Biomater. 9 (2013) 9243–9257.

[34] S. Goenka, V. Sant, S. Sant, Graphene-based nanomaterials for drug delivery and tissue engineering, J. Control. Release 173 (2014) 75–88.

[35] O. Erol, I. Uyan, M. Hatip, C. Yilmaz, A.B. Tekinay, M.O. Guler, Recent advances in bioactive 1D and 2D carbon nanomaterials for biomedical applications, Nanomedicine: NBM. (2017)https://doi.org/10.1016/j.nano.2017.03.021.

[36] J.M. Yoo, J.H. Kang, B.H. Hong, Graphene-based nanomaterials for versatile imaging studies, Chem. Soc. Rev. 44 (2015) 4835–4852.

[37] M. Karimi, A. Ghasemi, P. Sahandi Zangabad, R. Rahighi, S.M. Moosavi Basri, H. Mirshekari, M. Amiri, Z. Shafaei Pishabad, A. Aslani, M. Bozorgomid, D. Ghosh, A. Beyzavi, A. Vaseghi, A.R. Aref, L. Haghani, S. Bahrami, M.R. Hamblin, Smart micro/nanoparticles in stimulus-responsive drug/gene delivery systems, Chem. Soc. Rev. 45 (2016) 1457–1501.

[38] P. Zhang, C. Hu, W. Ran, J. Meng, Q. Yin, Y. Li, Recent progress in light-triggered nanotheranostics for cancer treatment, Theranostics. 6 (2016) 948–968.

[39] G. Shim, S. Ko, D. Kim, Q.-V. Le, G.T. Park, J. Lee, T. Kwon, H.-G. Choi, Y.B. Kim, Y.-K. Oh, Light-switchable systems for remotely controlled drug delivery, J. Control. Release 267 (2017) 67–79.

[40] Q. Yi, G.B. Sukhorukov, UV light stimulated encapsulation and release by polyelectrolyte microcapsules, Adv. Colloid Interf. Sci. 207 (2014) 280–289.

[41] R. Geetha Bai, N. Ninan, K. Muthoosamy, S. Manickam, Graphene: a versatile platform for nanotheranostics and tissue engineering, Prog. Mater. Sci. 91 (2018) 24–69.

[42] K. Yang, S. Zhang, G. Zhang, X. Sun, S.-T. Lee, Z. Liu, Graphene in mice: ultrahigh *in vivo* tumor uptake and efficient photothermal therapy, Nano Lett. 10 (2010) 3318–3323.

[43] J.T. Robinson, K. Welsher, S.M. Tabakman, S.P. Sherlock, H. Wang, R. Luong, H. Dai, High performance *in vivo* near-IR (> 1 μm) imaging and photothermal cancer therapy with carbon nanotubes, Nano Res. 3 (2010) 779–793.

[44] J.T. Robinson, S.M. Tabakman, Y. Liang, H. Wang, H. Sanchez Casalongue, D. Vinh, H. Dai, Ultrasmall reduced graphene oxide with high near-infrared absorbance for photothermal therapy, J. Am. Chem. Soc. 133 (2011) 6825–6831.

[45] O. Akhavan, E. Ghaderi, Graphene nanomesh promises extremely efficient *in vivo* photothermal therapy, Small 9 (2013) 3593–3601.

[46] L. Cheng, C. Wang, L. Feng, K. Yang, Z. Liu, Functional nanomaterials for phototherapies of cancer, Chem. Rev. 114 (2014) 10869–10939.

[47] B. Pegaz, E. Debefve, F. Borle, J.-P. Ballini, H. van den Bergh, Y.N. Kouakou-Konan, Encapsulation of porphyrins and chlorins in biodegradable nanoparticles: the effect of dye lipophilicity on the extravasation and the photothrombic activity. A comparative study, J. Photochem. Photobiol. B Biol. 80 (2005) 19–27.

[48] R. Bonnett, G. Martınez, Photobleaching of sensitisers used in photodynamic therapy, Tetrahedron 57 (2001) 9513–9547.

[49] A.M. Bugaj, Targeted photodynamic therapy – a promising strategy of tumor treatment, Photochem. Photobiol. Sci. 10 (2011) 1097–1109.

[50] J.P. Talreja, M. Degaetani, B.G. Sauer, M. Kahaleh, Photodynamic therapy for unresectable cholangiocarcinoma: contribution of single operator cholangioscopy for targeted treatment, Photochem. Photobiol. Sci. 10 (2011) 1233–1238.

[51] J. Chen, K. Stefflova, M.J. Niedre, B.C. Wilson, B. Chance, J.D. Glickson, G. Zheng, Protease-triggered photosensitizing beacon based on singlet oxygen quenching and activation, J. Am. Chem. Soc. 126 (2004) 11450–11451.

[52] H. Dong, Z. Zhao, H. Wen, F. Guo Li, A. Shen, F. Pilger, C. Lin, D. Shi, Poly(ethylene glycol) conjugated nano-graphene oxide for photodynamic therapy, Sci. China Chem. 53 (2010) 2265–2271.

[53] P. Huang, C. Xu, J. Lin, C. Wang, X. Wang, C. Zhang, X. Zhou, S. Guo, D. Cui, Folic acid-conjugated graphene oxide loaded with photosensitizers for targeting photodynamic therapy, Theranostics. 1 (2011) 240–250.

[54] F. Li, S.-J. Park, D. Ling, W. Park, J.Y. Han, K. Na, K. Char, Hyaluronic acid-conjugated graphene oxide/photosensitizer nanohybrids for cancer targeted photodynamic therapy, J. Mater. Chem. B 1 (2013) 1678–1686.

[55] D.E.J.G.J. Dolmans, D. Fukumura, R.K. Jain, Photodynamic therapy for cancer, Nat. Rev. Cancer 3 (2003) 380–387.

[56] Y. Wei, F. Zhou, D. Zhang, Q. Chen, D. Xing, A graphene oxide based smart drug delivery system for tumor mitochondria-targeting photodynamic therapy, Nanoscale 8 (2016) 3530–3538.

[57] Z. Liu, J.T. Robinson, X. Sun, H. Dai, PEGylated nanographene oxide for delivery of water-insoluble cancer drugs, J. Am. Chem. Soc. 130 (2008) 10876–10877.

[58] W. Zhang, Z. Guo, D. Huang, Z. Liu, X. Guo, H. Zhong, Synergistic effect of chemo-photothermal therapy using PEGylated graphene oxide, Biomaterials 32 (2011) 8555–8561.

[59] S.P. Sherlock, S.M. Tabakman, L. Xie, H. Dai, Photothermally enhanced drug delivery by ultrasmall multifunctional FeCo/graphitic shell nanocrystals, ACS Nano 5 (2011) 1505–1512.

[60] R. Kurapati, A.M. Raichur, Near-infrared light-responsive graphene oxide composite multilayer capsules: a novel route for remote controlled drug delivery, Chem. Commun. 49 (2013) 734–736.

[61] H. Kim, D. Lee, J. Kim, T. Kim, W.J. Kim, Photothermally triggered cytosolic drug delivery via endosome disruption using a functionalized reduced graphene oxide, ACS Nano 7 (2013) 6735–6746.

[62] J. Chen, H. Liu, C. Zhao, G. Qin, G. Xi, T. Li, X. Wang, T. Chen, One-step reduction and PEGylation of graphene oxide for photothermally controlled drug delivery, Biomaterials 35 (2014) 4986–4995.

[63] F. Yin, B. Gu, Y. Lin, N. Panwar, S.C. Tjin, J. Qu, S.P. Lau, K.-T. Yong, Functionalized 2D nanomaterials for gene delivery applications, Coord. Chem. Rev. 347 (2017) 77–97.

[64] L. Feng, S. Zhang, Z. Liu, Graphene based gene transfection, Nanoscale 3 (2011) 1252–1257.

[65] L. Feng, X. Yang, X. Shi, X. Tan, R. Peng, J. Wang, Z. Liu, Polyethylene glycol and polyethylenimine dual-functionalized nano-graphene oxide for photothermally enhanced gene delivery, Small 9 (2013) 1989–1997.

[66] H. Kim, W.J. Kim, Photothermally controlled gene delivery by reduced graphene oxide-polyethylenimine nanocomposite, Small 10 (2014) 117–126.

[67] B. Tian, C. Wang, S. Zhang, L. Feng, Z. Liu, Photothermally enhanced photodynamic therapy delivered by nano-graphene oxide, ACS Nano 5 (2011) 7000–7009.

[68] L. Feng, K. Li, X. Shi, M. Gao, J. Liu, Z. Liu, Smart pH-responsive nanocarriers based on nano-graphene oxide for combined chemo- and photothermal therapy overcoming drug resistance, Adv. Healthc. Mater. 3 (2014) 1261–1271.

[69] S.-H. Hu, R.-H. Fang, Y.-W. Chen, B.-J. Liao, I.-W. Chen, S.-Y. Chen, Photoresponsive protein-graphene-protein hybrid capsules with dual targeted heat-triggered drug delivery approach for enhanced tumor therapy, Adv. Funct. Mater. 24 (2014) 4144–4155.

[70] Y. Wang, K. Wang, J. Zhao, X. Liu, J. Bu, X. Yan, R. Huang, Multifunctional mesoporous silica-coated graphene nanosheet used for chemo-photothermal synergistic targeted therapy of glioma, J. Am. Chem. Soc. 135 (2013) 4799–4804.

[71] Y. Tang, H. Hu, M.G. Zhang, J. Song, L. Nie, S. Wang, G. Niu, P. Huang, G. Lu, X. Chen, An aptamer-targeting photoresponsive drug delivery system using "off–on" graphene oxide wrapped mesoporous silica nanoparticles, Nanoscale 7 (2015) 6304–6310.

[72] J. Bai, Y. Liu, X. Jiang, Multifunctional PEG-GO/CuS nanocomposites for near-infrared chemo-photothermal therapy, Biomaterials 35 (2014) 5805–5813.

[73] J. Shi, L. Wang, J. Zhang, R. Ma, J. Gao, Y. Liu, C. Zhang, Z. Zhang, A tumor-targeting near-infrared laser-triggered drug delivery system based on GO@Ag nanoparticles for chemo-photothermal therapy and X-ray imaging, Biomaterials 35 (2014) 5847–5861.

[74] J. Song, X. Yang, O. Jacobson, L. Lin, P. Huang, G. Niu, Q. Ma, X. Chen, Sequential drug release and enhanced photothermal and photoacoustic effect of hybrid reduced graphene oxide-loaded ultrasmall gold nanorod vesicles for cancer therapy, ACS Nano 9 (2015) 9199–9209.

[75] M.R. Junttila, F.J. de Sauvage, Influence of tumour micro-environment heterogeneity on therapeutic response, Nature 501 (2013) 346–354.

[76] S. Yoshida, S. Nakagawa, T. Yahara, T. Koga, H. Deguchi, K. Shirouzu, Relationship between microvessel density and thermographic hot areas in breast cancer, Surg. Today 33 (2003) 243–248.

[77] M. Tepper, A. Shoval, O. Hoffer, H. Confino, M. Schmidt, I. Kelson, Y. Keisari, I. Gannot, Thermographic investigation of tumor size, and its correlation to tumor relative temperature, in mice with transplantable solid breast carcinoma, J. Biomed. Opt. 18 (2013), 111410. .

[78] M. Karimi, P. Sahandi Zangabad, A. Ghasemi, M. Amiri, M. Bahrami, H. Malekzad, H. Ghahramanzadeh Asl, Z. Mahdieh, M. Bozorgomid, A. Ghasemi, M.R.R. Taji Boyuk, M.R. Hamblin, Temperature-responsive smart nanocarriers for delivery of therapeutic agents: applications and recent advances, ACS Appl. Mater. Interfaces 8 (2016) 21107–21133.

[79] H.G. Schild, Poly(*N*-isopropylacrylamide): experiment, theory and application, Prog. Polym. Sci. 17 (1992) 163–249.

[80] S. Sun, P. Wu, A one-step strategy for thermal- and pH-responsive graphene oxide interpenetrating polymer hydrogel networks, J. Mater. Chem. 21 (2011) 4095–4097.

[81] Y. Pan, H. Bao, N.G. Sahoo, T. Wu, L. Li, Water-soluble poly(*N*-isopropylacrylamide)-graphene sheets synthesized via click chemistry for drug delivery, Adv. Funct. Mater. 21 (2011) 2754–2763.

[82] L. Zhang, J. Xia, Q. Zhao, L. Liu, Z. Zhang, Functional graphene oxide as a nanocarrier for controlled loading and targeted delivery of mixed anticancer drugs, Small 6 (2010) 537–544.

[83] H. Wang, D. Sun, N. Zhao, X. Yang, Y. Shi, J. Li, Z. Su, G. Wei, Thermo-sensitive graphene oxide–polymer nanoparticle hybrids: synthesis, characterization, biocompatibility and drug delivery, J. Mater. Chem. B 2 (2014) 1362–1370.

[84] J. Yu, D.-Y. Huang, M.Z. Yousaf, Y.-L. Hou, S. Gao, Magnetic nanoparticle-based cancer therapy, Chinese Phys. B. 22 (2013), 27506. .

[85] N. Alegret, A. Criado, M. Prato, Recent advances of graphene-based hybrids with magnetic nanoparticles for biomedical applications, Curr. Med. Chem. 24 (2017) 529–536.

[86] X. Yang, X. Zhang, Y. Ma, Y. Huang, Y. Wang, Y. Chen, Superparamagnetic graphene oxide–Fe_3O_4 nanoparticles hybrid for controlled targeted drug carriers, J. Mater. Chem. 19 (2009) 2710–2713.

[87] X. Yang, Y. Wang, X. Huang, Y. Ma, Y. Huang, R. Yang, H. Duan, Y. Chen, Multi-functionalized graphene oxide based anticancer drug-carrier with dual-targeting function and pH-sensitivity, J. Mater. Chem. 21 (2011) 3448–3454.

[88] X. Fan, G. Jiao, L. Gao, P. Jin, X. Li, The preparation and drug delivery of a graphene–carbon nanotube–Fe_3O_4 nanoparticle hybrid, J. Mater. Chem. B 1 (2013) 2658–2664.

[89] O. Akhavan, A. Meidanchi, E. Ghaderi, S. Khoei, Zinc ferrite spinel-graphene in magneto-photothermal therapy of cancer, J. Mater. Chem. B 2 (2014) 3306–3314.

[90] J.-M. Shen, F.-Y. Gao, L.-P. Guan, W. Su, Y.-J. Yang, Q.-R. Li, Z.-C. Jin, Graphene oxide–Fe_3O_4 nanocomposite for combination of dual-drug chemotherapy with photothermal therapy, RSC Adv. 4 (2014) 18473–18484.

[91] H. Cong, J. He, Y. Lu, S. Yu, Water-soluble magnetic-functionalized reduced graphene oxide sheets: in situ synthesis and magnetic resonance imaging applications, Small 6 (2010) 169–173.

[92] W. Chen, P. Yi, Y. Zhang, L. Zhang, Z. Deng, Z. Zhang, Composites of aminodextran-coated Fe_3O_4 nanoparticles and graphene oxide for cellular magnetic resonance imaging, ACS Appl. Mater. Interfaces 3 (2011) 4085–4091.

[93] K. Yang, L. Hu, X. Ma, S. Ye, L. Cheng, X. Shi, C. Li, Y. Li, Z. Liu, Multimodal imaging guided photothermal therapy using functionalized graphene nanosheets anchored with magnetic nanoparticles, Adv. Mater. 24 (2012) 1868–1872.

[94] X. Ma, H. Tao, K. Yang, L. Feng, L. Cheng, X. Shi, Y. Li, L. Guo, Z. Liu, A functionalized graphene oxide-iron oxide nanocomposite for magnetically targeted drug delivery, photothermal therapy, and magnetic resonance imaging, Nano Res. 5 (2012) 199–212.

[95] X. Shi, H. Gong, Y. Li, C. Wang, L. Cheng, Z. Liu, Graphene-based magnetic plasmonic nanocomposite for dual bioimaging and photothermal therapy, Biomaterials 34 (2013) 4786–4793.

[96] G. Wang, G. Chen, Z. Wei, X. Dong, M. Qi, Multifunctional Fe_3O_4/graphene oxide nanocomposites for magnetic resonance imaging and drug delivery, Mater. Chem. Phys. 141 (2013) 997–1004.

[97] M. Zhang, Y. Cao, Y. Chong, Y. Ma, H. Zhang, Z. Deng, C. Hu, Z. Zhang, Graphene oxide based theranostic platform for T_1-weighted magnetic resonance imaging and drug delivery, ACS Appl. Mater. Interfaces 5 (2013) 13325–13332.

[98] G. Fu, L. Zhu, K. Yang, R. Zhuang, J. Xie, F. Zhang, Diffusion-weighted magnetic resonance imaging for therapy response monitoring and early treatment prediction of photothermal therapy, ACS Appl. Mater. Interfaces 8 (2016) 5137–5147.

[99] X. Zhu, H. Zhang, H. Huang, Y. Zhang, L. Hou, Z. Zhang, Functionalized graphene oxide-based thermosensitive hydrogel for magnetic hyperthermia therapy on tumors, Nanotechnology 26 (2015), 365103. .

[100] A.K. Swain, L. Pradhan, D. Bahadur, Polymer stabilized Fe_3O_4-graphene as an amphiphilic drug carrier for thermo-chemotherapy of cancer, ACS Appl. Mater. Interfaces 7 (2015) 8013–8022.

[101] L. Deng, Q. Li, S. Al-Rehili, H. Omar, A. Almalik, A. Alshamsan, J. Zhang, N.M. Khashab, Hybrid iron oxide–graphene oxide–polysaccharides microcapsule: a micro-matryoshka for on-demand drug release and antitumor therapy *in vivo*, ACS Appl. Mater. Interfaces 8 (2016) 6859–6868.

[102] Q. Zhang, Z. Wu, N. Li, Y. Pu, B. Wang, T. Zhang, J. Tao, Advanced review of graphene-based nanomaterials in drug delivery systems: synthesis, modification, toxicity and application, Mater. Sci. Eng. C. 77 (2017) 1363–1375.

[103] Y. Zhao, A.C. Tavares, M.A. Gauthier, Nano-engineered electro-responsive drug delivery systems, J. Mater. Chem. B 4 (2016) 3019–3030.

[104] A. Servant, V. Leon, D. Jasim, L. Methven, P. Limousin, E.V. Fernandez-Pacheco, M. Prato, K. Kostarelos, Graphene-based electroresponsive scaffolds as polymeric implants for on-demand drug delivery, Adv. Healthc. Mater. 3 (2014) 1334–1343.

[105] C.L. Weaver, J.M. Larosa, X. Luo, X.T. Cui, Electrically controlled drug delivery from graphene oxide nanocomposite films, ACS Nano 8 (2014) 1834–1843.

[106] N. Mac Kenna, P. Calvert, A. Morrin, G.G. Wallace, S.E. Moulton, Electro-stimulated release from a reduced graphene oxide composite hydrogel, J. Mater. Chem. B 3 (2015) 2530–2537.

[107] Y. Chen, P. Xu, Z. Shu, M. Wu, L. Wang, S. Zhang, Y. Zheng, H. Chen, J. Wang, Y. Li, J. Shi, Multifunctional graphene oxide-based triple stimuli-responsive nanotheranostics, Adv. Funct. Mater. 24 (2014) 4386–4396.

[108] C. Tan, Z. Lai, H. Zhang, Ultrathin two-dimensional multinary layered metal chalcogenide nanomaterials, Adv. Mater. 29 (2017), 1701392. .

[109] S.S. Chou, B. Kaehr, J. Kim, B.M. Foley, M. De, P.E. Hopkins, J. Huang, C.J. Brinker, V.P. Dravid, Chemically exfoliated MoS_2 as near-infrared photothermal agents, Angew. Chem. Int. Ed. 52 (2013) 4160–4164.

[110] S. Wang, X. Li, Y. Gong, X. Zhou, H. Jin, H. Yan, J. Liu, Facile synthesis of soybean phospholipid-encapsulated MoS_2 nanosheets for efficient *in vitro* and *in vivo* photothermal regression of breast tumor, Int. J. Nanomedicine 11 (2016) 1819–1833.

[111] S. Wang, K. Li, Y. Chen, H. Chen, M. Ma, J. Feng, Q. Zhao, J. Shi, Biocompatible PEGylated MoS_2 nanosheets: controllable bottom-up synthesis and highly efficient photothermal regression of tumor, Biomaterials 39 (2015) 206–217.

[112] L. Chen, Y. Feng, X. Zhou, Q. Zhang, W. Nie, W. Wang, Y. Zhang, C. He, One-pot synthesis of MoS_2 nanoflakes with desirable degradability for photothermal cancer therapy, ACS Appl. Mater. Interfaces 9 (2017) 17347–17358.

[113] L. Cheng, J. Liu, X. Gu, H. Gong, X. Shi, T. Liu, C. Wang, X. Wang, G. Liu, H. Xing, W. Bu, B. Sun, Z. Liu, PEGylated WS_2 nanosheets as a multifunctional theranostic agent for *in vivo* dual-modal CT/photoacoustic imaging guided photothermal therapy, Adv. Mater. 26 (2014) 1886–1893.

[114] Q. Liu, C. Sun, Q. He, A. Khalil, T. Xiang, D. Liu, Y. Zhou, J. Wang, L. Song, Stable metallic 1T-WS_2 ultrathin nanosheets as a promising agent for near-infrared photothermal ablation cancer therapy, Nano Res. 8 (2015) 3982–3991.

[115] Z. Lei, Y. Zhou, P. Wu, Simultaneous exfoliation and functionalization of $MoSe_2$ nanosheets to prepare "smart" nanocomposite hydrogels with tunable dual stimuli-responsive behavior, Small 12 (2016) 3112–3118.

[116] H. Chen, T. Liu, Z. Su, L. Shang, G. Wei, 2D transition metal dichalcogenide nanosheets for photo/thermo-based tumor imaging and therapy, Nanoscale Horizons. 3 (2018) 74–89.

[117] Z. Lei, W. Zhu, S. Xu, J. Ding, J. Wan, P. Wu, Hydrophilic $MoSe_2$ nanosheets as effective photothermal therapy agents and their application in smart devices, ACS Appl. Mater. Interfaces 8 (2016) 20900–20908.

[118] L. Yuwen, J. Zhou, Y. Zhang, Q. Zhang, J. Shan, Z. Luo, L. Weng, Z. Teng, L. Wang, Aqueous phase preparation of ultrasmall $MoSe_2$ nanodots for efficient photothermal therapy of cancer cells, Nanoscale 8 (2016) 2720–2726.

[119] C. Wang, J. Bai, Y. Liu, X. Jia, X. Jiang, Polydopamine coated selenide molybdenum: a new photothermal nanocarrier for highly effective chemo-photothermal synergistic therapy, ACS Biomater. Sci. Eng. 2 (2016) 2011–2017.

[120] C. Zhong, X. Zhao, L. Wang, Y. Li, Y. Zhao, Facile synthesis of biocompatible $MoSe_2$ nanoparticles for efficient targeted photothermal therapy of human lung cancer, RSC Adv. 7 (2017) 7382–7391.

[121] J. Li, F. Jiang, B. Yang, X. Song, Y. Liu, H. Yang, D. Cao, W.-R. Shi, G.-N. Chen, Topological insulator bismuth selenide as a theranostic platform for simultaneous cancer imaging and therapy, Sci. Rep. 3 (2013) 1998.

[122] Z. Li, J. Shao, Q. Luo, X.-F. Yu, H. Xie, H. Fu, S. Tang, H. Wang, G. Han, P.K. Chu, Cell-borne 2D nanomaterials for efficient cancer targeting and photothermal therapy, Biomaterials 133 (2017) 37–48.

[123] Y. Zhao, L. Tong, Z. Li, N. Yang, H. Fu, L. Wu, H. Cui, W. Zhou, J. Wang, H. Wang, P.K. Chu, X.-F. Yu, Stable and multifunctional dye-modified black phosphorus

nanosheets for near-infrared imaging-guided photothermal therapy, Chem. Mater. 29 (2017) 7131–7139.
[124] M. Naguib, M. Kurtoglu, V. Presser, J. Lu, J. Niu, M. Heon, L. Hultman, Y. Gogotsi, M.W. Barsoum, Two-dimensional nanocrystals produced by exfoliation of Ti_3AlC_2, Adv. Mater. 23 (2011) 4248–4253.
[125] J. Zeng, D. Goldfeld, Y. Xia, A plasmon-assisted optofluidic (PAOF) system for measuring the photothermal conversion efficiencies of gold nanostructures and controlling an electrical switch, Angew. Chem. Int. Ed. 52 (2013) 4169–4173.
[126] H. Lin, X. Wang, L. Yu, Y. Chen, J. Shi, Two-dimensional ultrathin MXene ceramic nanosheets for photothermal conversion, Nano Lett. 17 (2017) 384–391.
[127] C. Dai, H. Lin, G. Xu, Z. Liu, R. Wu, Y. Chen, Biocompatible 2D titanium carbide (MXenes) composite nanosheets for pH-responsive MRI-guided tumor hyperthermia, Chem. Mater. 29 (2017) 8637–8652.
[128] Z. Ma, M. Zhang, X. Jia, J. Bai, Y. Ruan, C. Wang, X. Sun, X. Jiang, Fe^{III}-doped two-dimensional C_3N_4 nanofusiform: a new O_2-evolving and mitochondria-targeting photodynamic agent for MRI and enhanced antitumor therapy, Small 12 (2016) 5477–5487.
[129] L. Lin, Z. Cong, J. Li, K. Ke, S. Guo, H. Yang, G. Chen, Graphitic-phase C_3N_4 nanosheets as efficient photosensitizers and pH-responsive drug nanocarriers for cancer imaging and therapy, J. Mater. Chem. B 2 (2014) 1031–1037.
[130] H. Wang, X. Yang, W. Shao, S. Chen, J. Xie, X. Zhang, J. Wang, Y. Xie, Ultrathin black phosphorus nanosheets for efficient singlet oxygen generation, J. Am. Chem. Soc. 137 (2015) 11376–11382.
[131] H. Wan, Y. Zhang, W. Zhang, H. Zou, Robust two-photon visualized nanocarrier with dual targeting ability for controlled chemo-photodynamic synergistic treatment of cancer, ACS Appl. Mater. Interfaces 7 (2015) 9608–9618.
[132] R. Chen, J. Zhang, Y. Wang, X. Chen, J.A. Zapien, C.-S. Lee, Graphitic carbon nitride nanosheet@metal–organic framework core–shell nanoparticles for photo-chemo combination therapy, Nanoscale 7 (2015) 17299–17305.
[133] D. Ji, Y. Zhang, Y. Zang, J. Li, G. Chen, X. He, H. Tian, Targeted intracellular production of reactive oxygen species by a 2D molybdenum disulfide glycosheet, Adv. Mater. 28 (2016) 9356–9363.
[134] D.-K. Ji, G.-R. Chen, X.-P. He, H. Tian, Simultaneous detection of diverse glycoligand-receptor recognitions using a single-excitation, dual-emission graphene composite, Adv. Funct. Mater. 25 (2015) 3483–3487.
[135] T. Liu, C. Wang, X. Gu, H. Gong, L. Cheng, X. Shi, L. Feng, B. Sun, Z. Liu, Drug delivery with PEGylated MoS_2 nano-sheets for combined photothermal and chemotherapy of cancer, Adv. Mater. 26 (2014) 3433–3440.
[136] W. Yin, L. Yan, J. Yu, G. Tian, L. Zhou, X. Zheng, X. Zhang, Y. Yong, J. Li, Z. Gu, Y. Zhao, High-throughput synthesis of single-layer MoS_2 nanosheets as a near-infrared photothermal-triggered drug delivery for effective cancer therapy, ACS Nano 8 (2014) 6922–6933.
[137] S. Wang, Y. Chen, X. Li, W. Gao, L. Zhang, J. Liu, Y. Zheng, H. Chen, J. Shi, Injectable 2D MoS_2-integrated drug delivering implant for highly efficient NIR-triggered synergistic tumor hyperthermia, Adv. Mater. 27 (2015) 7117–7122.
[138] G. Yang, H. Gong, T. Liu, X. Sun, L. Cheng, Z. Liu, Two-dimensional magnetic WS_2@Fe_3O_4 nanocomposite with mesoporous silica coating for drug delivery and imaging-guided therapy of cancer, Biomaterials 60 (2015) 62–71.
[139] L. Kong, L. Xing, B. Zhou, L. Du, X. Shi, Dendrimer-modified MoS_2 nanoflakes as a platform for combinational gene silencing and photothermal therapy of tumors, ACS Appl. Mater. Interfaces 9 (2017) 15995–16005.
[140] C. Zhang, Y. Yong, L. Song, X. Dong, X. Zhang, X. Liu, Z. Gu, Y. Zhao, Z. Hu, Multifunctional WS_2@poly(ethylene imine) nanoplatforms for imaging guided gene-photothermal synergistic therapy of cancer, Adv. Healthc. Mater. 5 (2016) 2776–2787.
[141] J. Kim, H. Kim, W.J. Kim, Single-layered MoS_2-PEI-PEG nanocomposite-mediated gene delivery controlled by photo and redox stimuli, Small 12 (2016) 1184–1192.
[142] Y. Yong, L. Zhou, Z. Gu, L. Yan, G. Tian, X. Zheng, X. Liu, X. Zhang, J. Shi, W. Cong, W. Yin, Y. Zhao, WS_2 nanosheet as a new photosensitizer carrier for combined photodynamic and photothermal therapy of cancer cells, Nanoscale 6 (2014) 10394–10403.
[143] T. Liu, C. Wang, W. Cui, H. Gong, C. Liang, X. Shi, Z. Li, B. Sun, Z. Liu, Combined photothermal and photodynamic therapy delivered by PEGylated MoS_2 nanosheets, Nanoscale 6 (2014) 11219–11225.
[144] L. Liu, J. Wang, X. Tan, X. Pang, Q. You, Q. Sun, F. Tan, N. Li, Photosensitizer loaded PEG-MoS_2–au hybrids for CT/NIRF imaging-guided stepwise photothermal and photodynamic therapy, J. Mater. Chem. B 5 (2017) 2286–2296.
[145] R. Anbazhagan, Y.-A. Su, H.-C. Tsai, R.-J. Jeng, MoS_2–Gd chelate magnetic nanomaterials with core–shell structure used as contrast agents *in vivo* magnetic resonance imaging, ACS Appl. Mater. Interfaces 8 (2016) 1827–1835.
[146] J. Yu, W. Yin, X. Zheng, G. Tian, X. Zhang, T. Bao, X. Dong, Z. Wang, Z. Gu, X. Ma, Y. Zhao, Smart MoS_2/Fe_3O_4 nanotheranostic for magnetically targeted photothermal therapy guided by magnetic resonance/photoacoustic imaging, Theranostics. 5 (2015) 931–945.
[147] X. Qian, S. Shen, T. Liu, L. Cheng, Z. Liu, Two-dimensional TiS_2 nanosheets for *in vivo* photoacoustic imaging and photothermal cancer therapy, Nanoscale 7 (2015) 6380–6387.
[148] X. Meng, Z. Liu, Y. Cao, W. Dai, K. Zhang, H. Dong, X. Feng, X. Zhang, Fabricating aptamer-conjugated PEGylated-MoS_2/$Cu_{1.8}S$ theranostic nanoplatform for multiplexed imaging diagnosis and chemo-photothermal therapy of cancer, Adv. Funct. Mater. 27 (2017), 1605592. .
[149] M. Chen, X. Qin, G. Zeng, Biodegradation of carbon nanotubes, graphene, and their derivatives, Trends Biotechnol. 35 (2017) 836–846.
[150] A. Bianco, Graphene: safe or toxic? The two faces of the medal, Angew. Chem. Int. Ed. 52 (2013) 4986–4997.
[151] K. Yang, Y. Li, X. Tan, R. Peng, Z. Liu, Behavior and toxicity of graphene and its functionalized derivatives in biological systems, Small 9 (2013) 1492–1503.
[152] S.K. Singh, M.K. Singh, P.P. Kulkarni, V.K. Sonkar, J.J.A. Grácio, D. Dash, Amine-modified graphene: thrombo-protective safer alternative to graphene oxide for biomedical applications, ACS Nano 6 (2012) 2731–2740.
[153] M.C. Duch, G.R.S. Budinger, Y.T. Liang, S. Soberanes, D. Urich, S.E. Chiarella, L.A. Campochiaro, A. Gonzalez, N.S. Chandel, M.C. Hersam, G.M. Mutlu, Minimizing oxidation and stable nanoscale dispersion improves the biocompatibility of graphene in the lung, Nano Lett. 11 (2011) 5201–5207.
[154] X. Zhang, J. Yin, C. Peng, W. Hu, Z. Zhu, W. Li, C. Fan, Q. Huang, Distribution and biocompatibility studies of graphene oxide in mice after intravenous administration, Carbon 49 (2011) 986–995.
[155] R. Kurapati, J. Russier, M.A. Squillaci, E. Treossi, C. Ménard-Moyon, A.E. Del Rio-Castillo, E. Vazquez, P. Samorì, V. Palermo, A. Bianco, Dispersibility-dependent biodegradation of graphene oxide by myeloperoxidase, Small 11 (2015) 3985–3994.
[156] C.M. Girish, A. Sasidharan, G.S. Gowd, S. Nair, M. Koyakutty, Confocal Raman imaging study showing macrophage mediated biodegradation of graphene *in vivo*, Adv. Healthc. Mater. 2 (2013) 1489–1500.
[157] R. Kurapati, L. Muzi, A.P.R. de Garibay, J. Russier, D. Voiry, I.A. Vacchi, M. Chhowalla, A. Bianco, Enzymatic biodegradability of pristine and functionalized transition metal dichalcogenide MoS_2 nanosheets, Adv. Funct. Mater. 27 (2017), 1605176. .
[158] Y. Zhang, D. Meng, J. Shi, Z. Zhang, Y. Hao, L. Wang, B. Zhang, D. Li, H. Zhang, Manganese dioxide nanosheets-based redox/pH-responsive drug delivery system for cancer theranostic application, Int. J. Nanomedicine 11 (2016) 1759–1778.
[159] Y. Chen, D. Ye, M. Wu, H. Chen, L. Zhang, J. Shi, L. Wang, Break-up of two-dimensional MnO_2 nanosheets promotes ultrasensitive pH-triggered theranostics of cancer, Adv. Mater. 26 (2014) 7019–7026.
[160] W. Tao, X. Zhu, X. Yu, X. Zeng, Q. Xiao, X. Zhang, X. Ji, X. Wang, J. Shi, H. Zhang, L. Mei, Black phosphorus nanosheets as a robust delivery platform for cancer theranostics, Adv. Mater. 29 (2017) 1603276.
[161] K. Yang, J. Wan, S. Zhang, B. Tian, Y. Zhang, Z. Liu, The influence of surface chemistry and size of nanoscale graphene oxide on photothermal therapy of cancer using ultra-low laser power, Biomaterials 33 (2012) 2206–2214.
[162] D.-K. Ji, Y. Zhang, X.-P. He, G.-R. Chen, An insight into graphene oxide associated fluorogenic sensing of glycodye–lectin interactions, J. Mater. Chem. B 3 (2015) 6656–6661.
[163] C. Liang, L. Xu, G. Song, Z. Liu, Emerging nanomedicine approaches fighting tumor metastasis: animal models, metastasis-targeted drug delivery, phototherapy, and immunotherapy, Chem. Soc. Rev. 45 (2016) 6250–6269.
[164] Q. Fan, Z. Chen, C. Wang, Z. Liu, Toward biomaterials for enhancing immune checkpoint blockade therapy, Adv. Funct. Mater. (2018)https://doi.org/10.1002/adfm.201802540.
[165] D.J. Irvine, M.C. Hanson, K. Rakhra, T. Tokatlian, Synthetic nanoparticles for vaccines and immunotherapy, Chem. Rev. 115 (2015) 11109–11146.
[166] J. Nam, S. Son, L.J. Ochyl, R. Kuai, A. Schwendeman, J.J. Moon, Chemo-photothermal therapy combination elicits anti-tumor immunity against advanced metastatic cancer, Nat. Commun. 9 (2018) 1074.
[167] Y. Liu, P. MacCarini, G.M. Palmer, W. Etienne, Y. Zhao, C.T. Lee, X. Ma, B.A. Inman, T. Vo-Dinh, Synergistic immuno photothermal nanotherapy (SYMPHONY) for the treatment of unresectable and metastatic cancers, Sci. Rep. 7 (2017) 8606.
[168] Y. Tao, E. Ju, Z. Liu, K. Dong, J. Ren, X. Qu, Engineered, self-assembled near-infrared photothermal agents for combined tumor immunotherapy and chemo-photothermal therapy, Biomaterials 35 (2014) 6646–6656.